Supporting Information

Opioid Receptor Probes Derived from Cycloaddition of the Hallucinogen Natural Product Salvinorin A

*Anthony Lozama, Christopher W. Cunningham, Michael J. Caspers, Justin T. Douglas, Christina M. Dersch, Richard B. Rothman, and Thomas E. Prisinzano**

Contents of Supporting Information

Table S1. Calculated dihedral angles and predicted $^{3}J_{H,H}$ constants for all possible configurations of **12**.

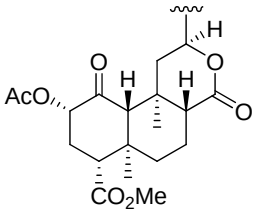

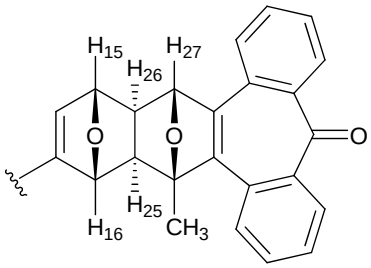

endo,endo

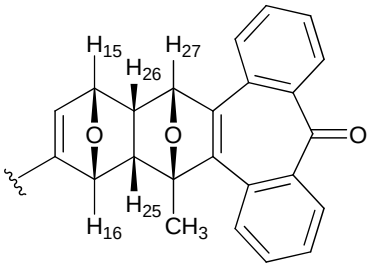

exo,exo

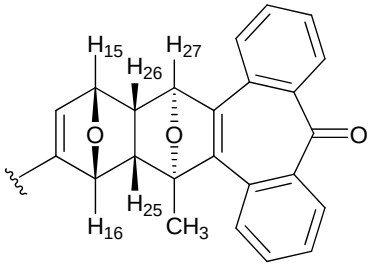

endo,exo

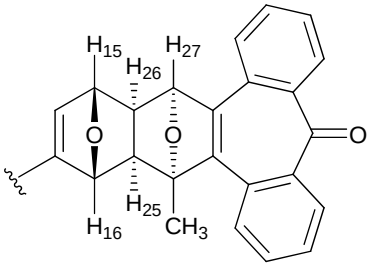

exo,endo

	Dihedral angle (predicted $^3J_{H,H}$) [a,b]				**Actual $^3J_{H,H}$**
	endo,endo	*exo,exo*	*endo,exo*	*exo,endo*	**12**
H16-C16-C25-**H25**	80.4 (1.43)	320.3 (5.15)	319.7 (5.07)	83.4 (1.38)	m (H-16)
H15-C15-C26-**H26**	297.2 (2.52)	34.2 (5.80)	32.6 (5.98)	281.0 (1.47)	dd, 4.6 and 1.6 (H-15)
H26-C26-C27-**H27**	82.5 (1.39)	320.2 (5.14)	274.9 (1.36)	37.3 (5.44)	s (H-27)
H26-C26-C25-**H25**	356.6 (8.03)	6.6 (7.96)	6.6 (7.96)	357.5 (8.05)	m (H-26)

[a]Dihedral angles (Θ) given in degrees, $^3J_{H,H}$ given in Hz. [b]Dihedral angles were calculated according to the following method: models of derivatives of **12** were generated using SYBYL8.0 and subjected to five iterations of energy minimization, followed by molecular dynamics (MD) simulations. Models were minimized to a gradient of 0.05 kcal/molÅ. MD simulations were performed over a period of 1000fs at 300K using the Tripos force field and application of Gasteiger-Hückel charges. This method was used to approximate the global minimum energy conformation of each derivative. After calculating the Θ values for appropriate H-H partners, predicted $^3J_{H,H}$ coupling values were predicted using the Karplus equation ($J = A - B\cos\Theta + C\cos\Theta$, with A = 7.76, B = -1.1, C = 1.4). From the ^{1}H NMR spectrum of **12**, H-15 was found to exhibit $^3J_{H,H}$ constants of 4.6 and 1.6 (to H-26 and H-14, respectively). Based on the value of 4.6 for H-15 with H-26, configurations *endo,endo* and *exo,endo* were eliminated. $^3J_{H,H}$ values for H-16, H-25, and H-26 were unable to be determined, as these existed as multiplets. The peak for H-27 appeared as a singlet, however, indicating only a very small coupling with H-26. The predicted $^3J_{H,H}$ between H-26 and H-27 for *exo,exo* (5.14) is much greater than that predicted for *endo,exo* (1.36), suggesting that the overall conformation of this ring system is *endo,exo*, supporting previous findings (see Ref. 40).

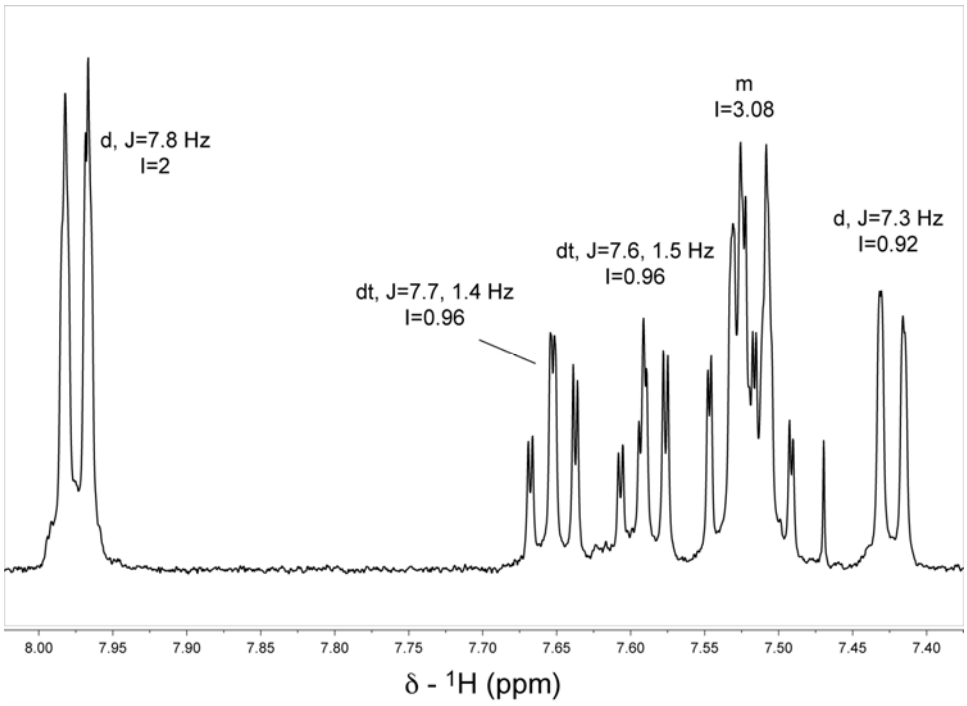

Figure S1 Aromatic ^{1}H NMR region of **12** labeled with splitting pattern, scalar coupling values and integrals.

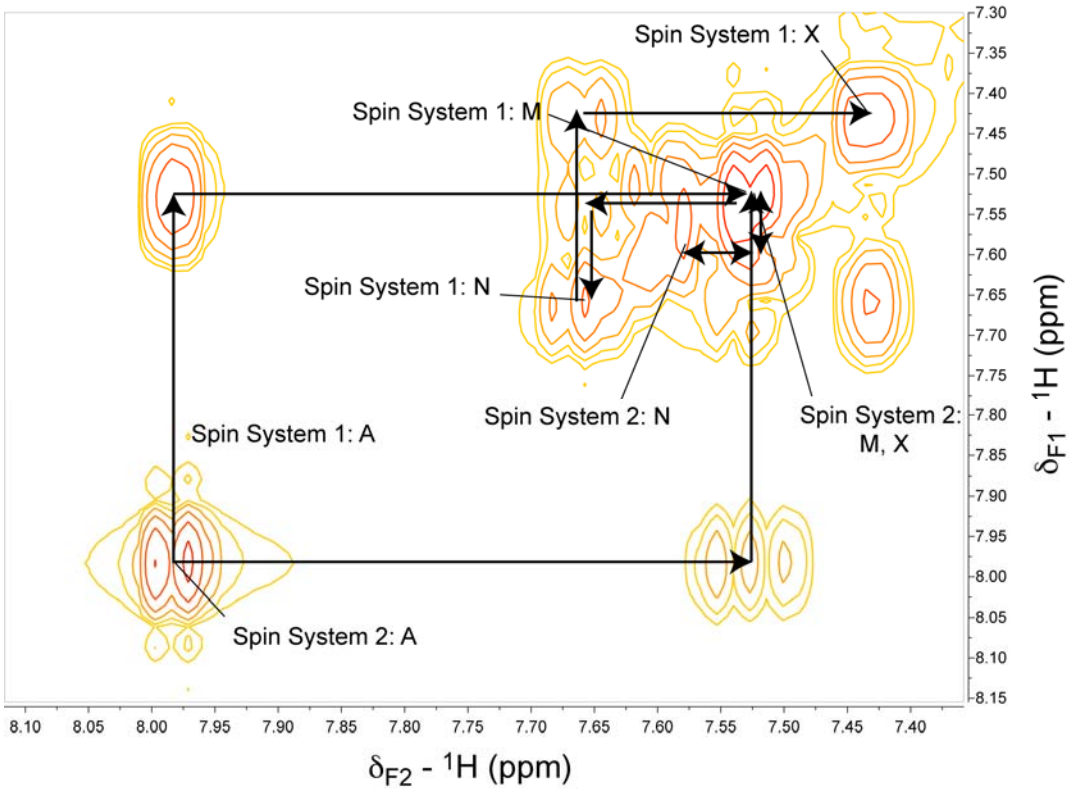

Figure S2. Aromatic region of 2D COSY spectrum of **12**. The walk through spin system 1 and 2 is denoted on the upper and lower diagonal, respectively.

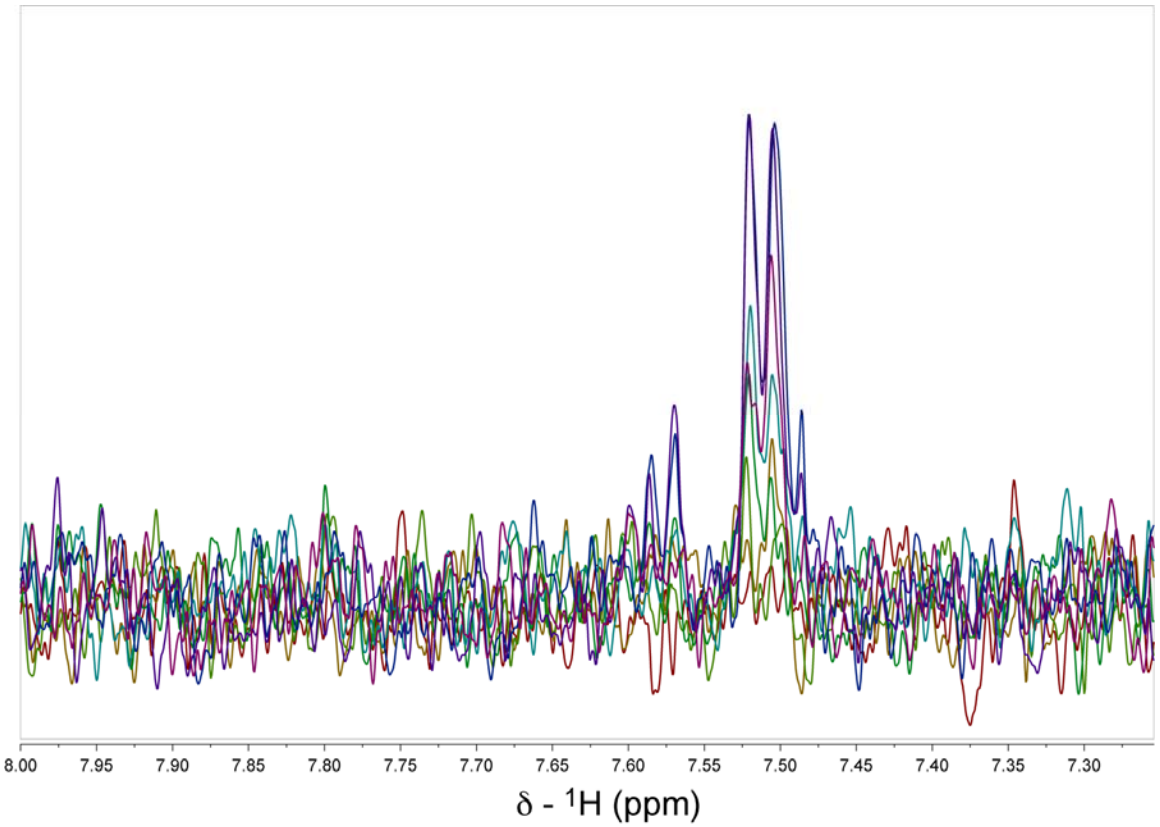

Figure S3. Overlay of selective 1D ^{1}H ROE with mixing time of 5 μs (red), 25 ms (gold), 50 ms (green), 100 ms (brown), 200 ms (cyan), 500 ms (blue), 1000 ms (purple) and 2000 ms (pink) following selective excitation of resonance at 1.7 ppm using excitation sculpting. This resonance corresponds to the methyl protons from atom number 43. Magnetization is transfer to X (7.52 ppm) and N (7.59 ppm) resonances of spin system 2, exclusively.

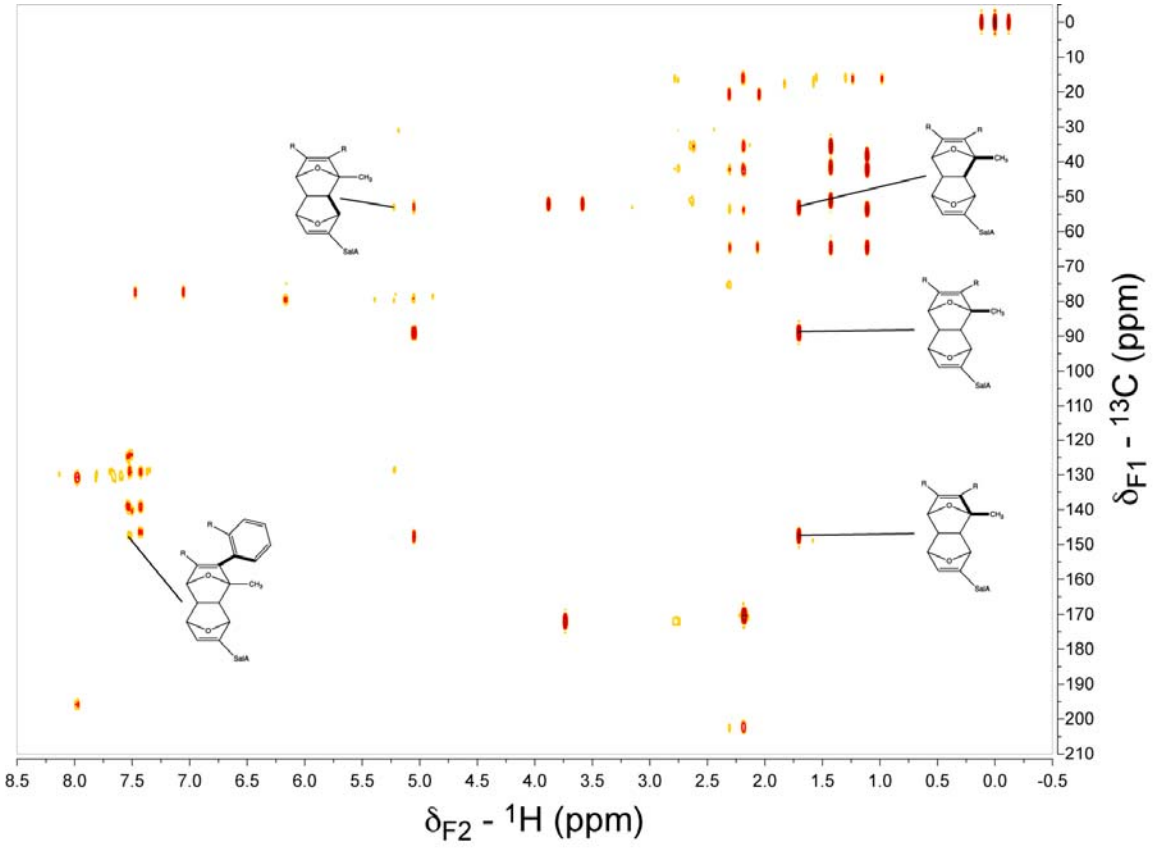

Figure S4. HMBC of **12**. Correlations that establish the regiochemistry of **12**. 2D 1H-13C HMBC of **12**. Correlations that establish the regiochemistry of **12** are labeled by the moiety of **12**. The specific 2 or 3 bond $^{1}H - ^{13}C$ coupling is in bold.

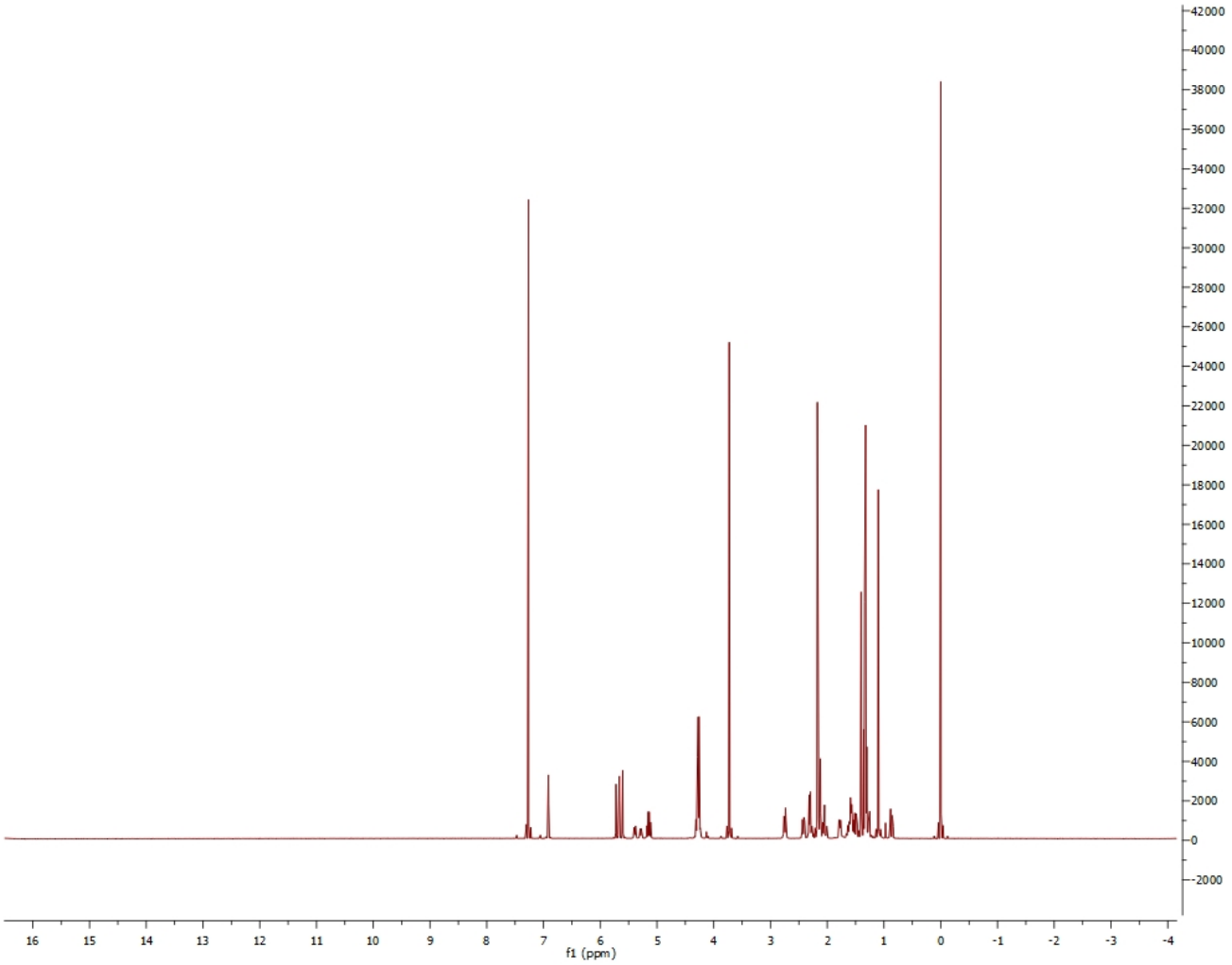

Figure S5. ^{1}H Spectrum of **5**.

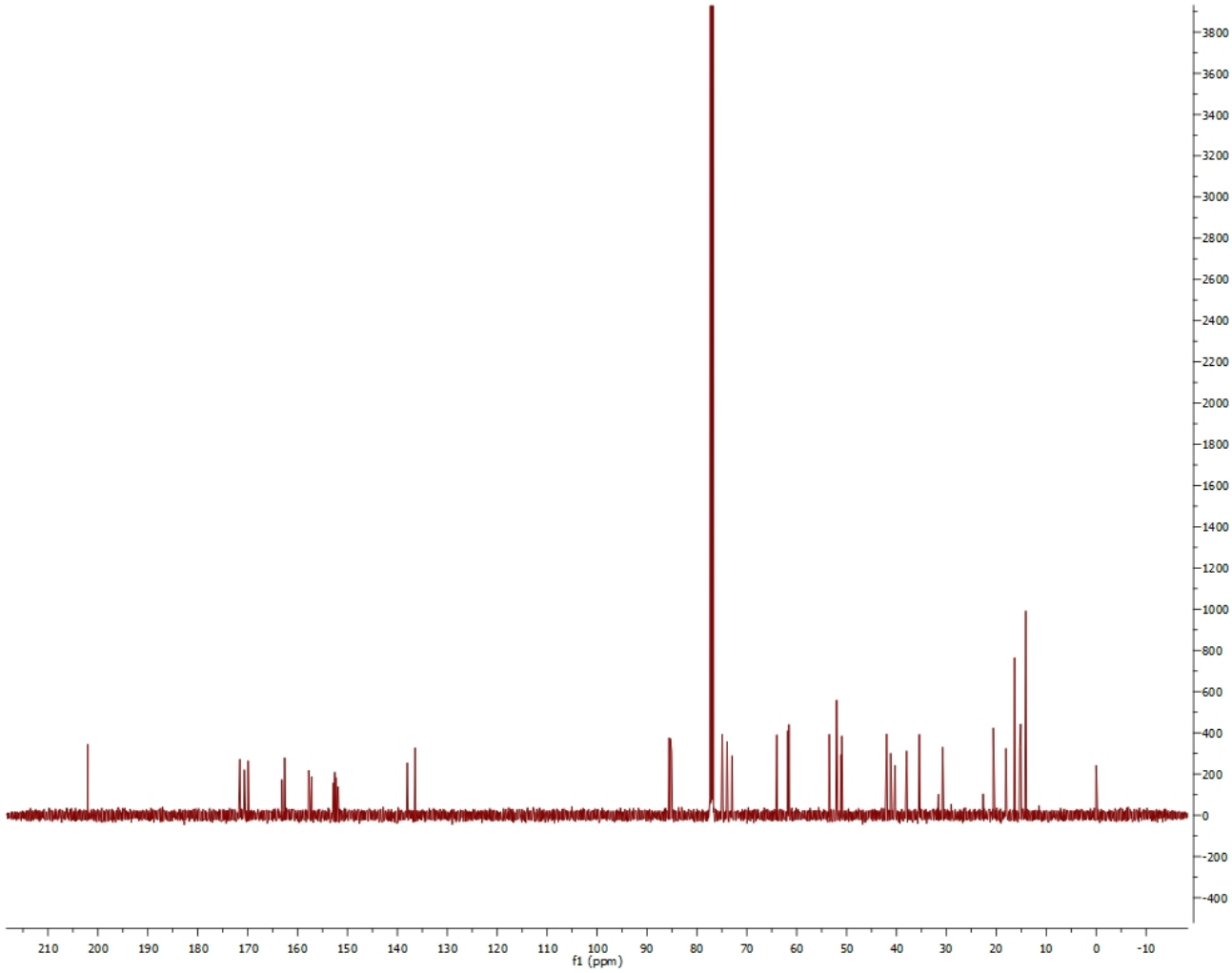

Figure S6. ^{13}C Spectrum of **5**.

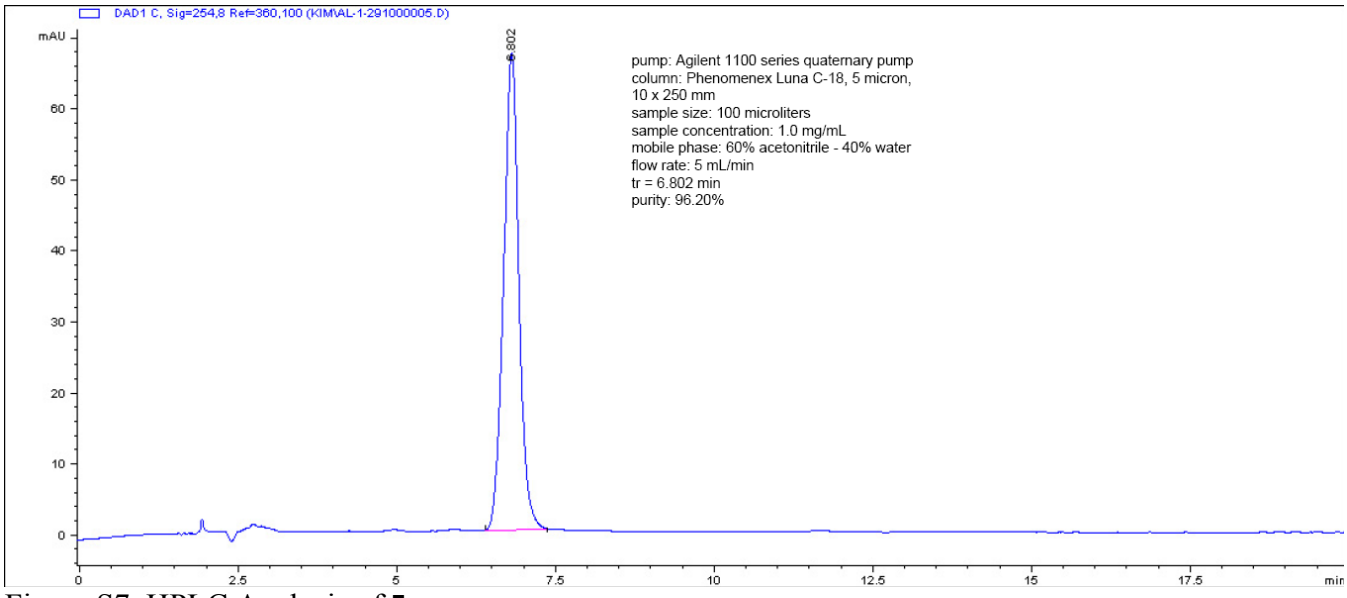

Figure S7. HPLC Analysis of **5**.

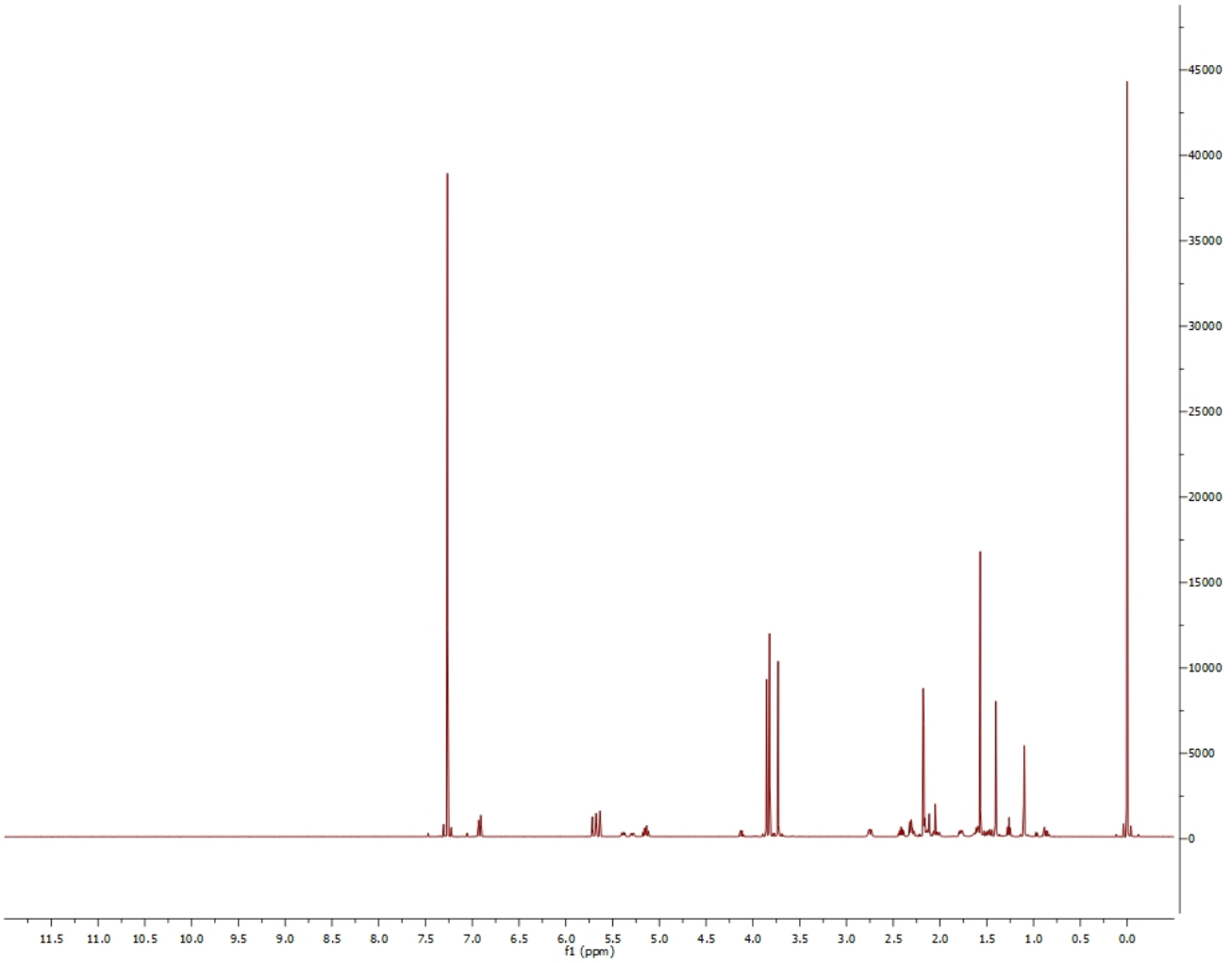

Figure S8. ^{1}H Spectrum of **6**.

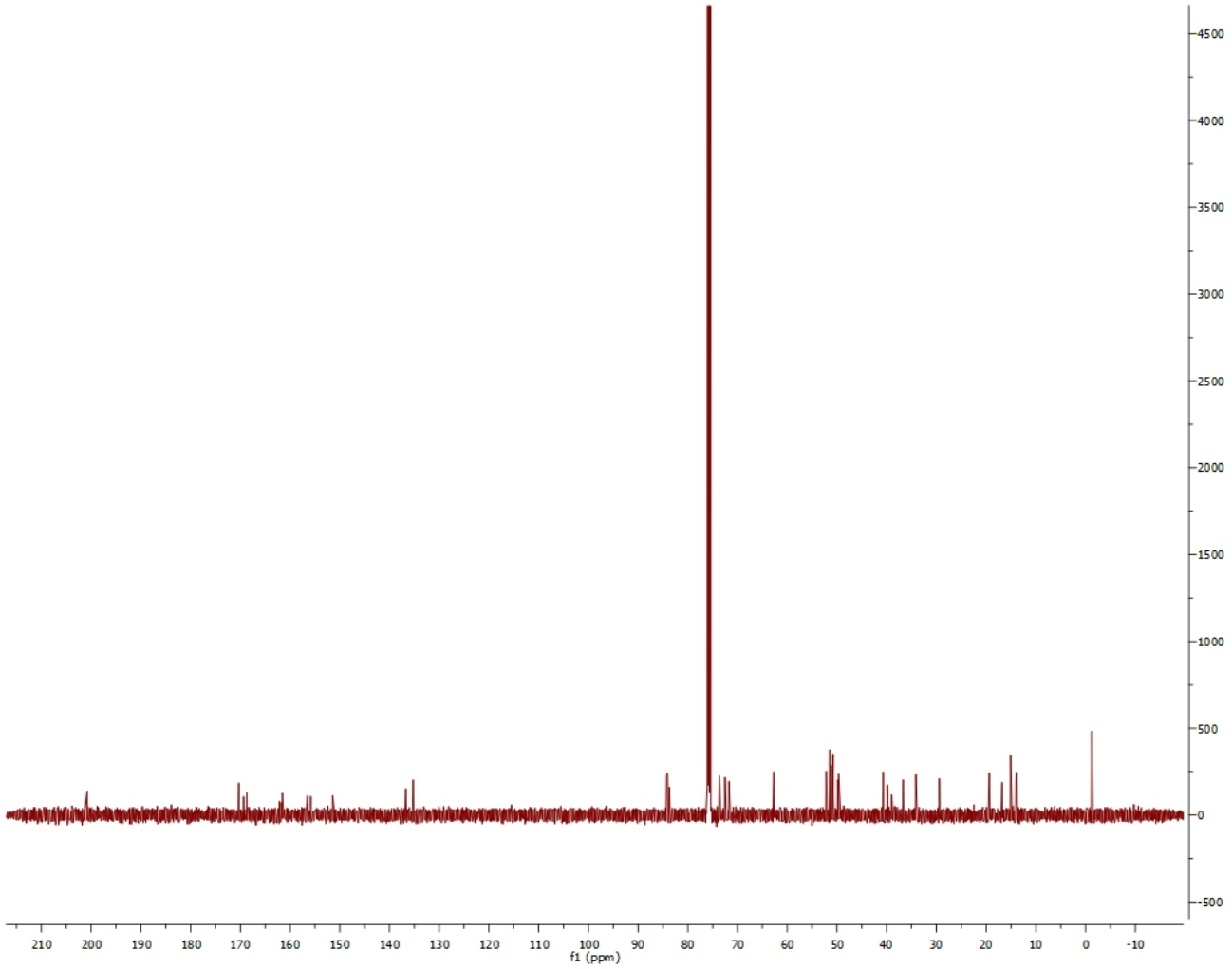

Figure S9. ^{13}C Spectrum of **6**.

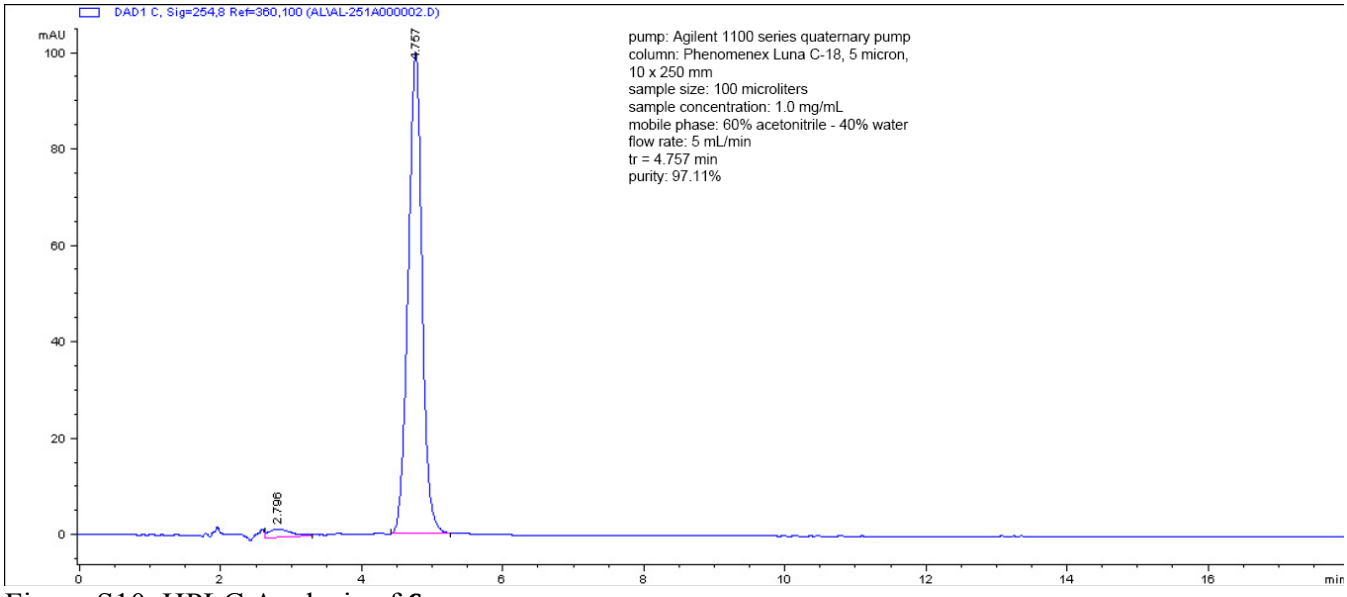

Figure S10. HPLC Analysis of **6**.

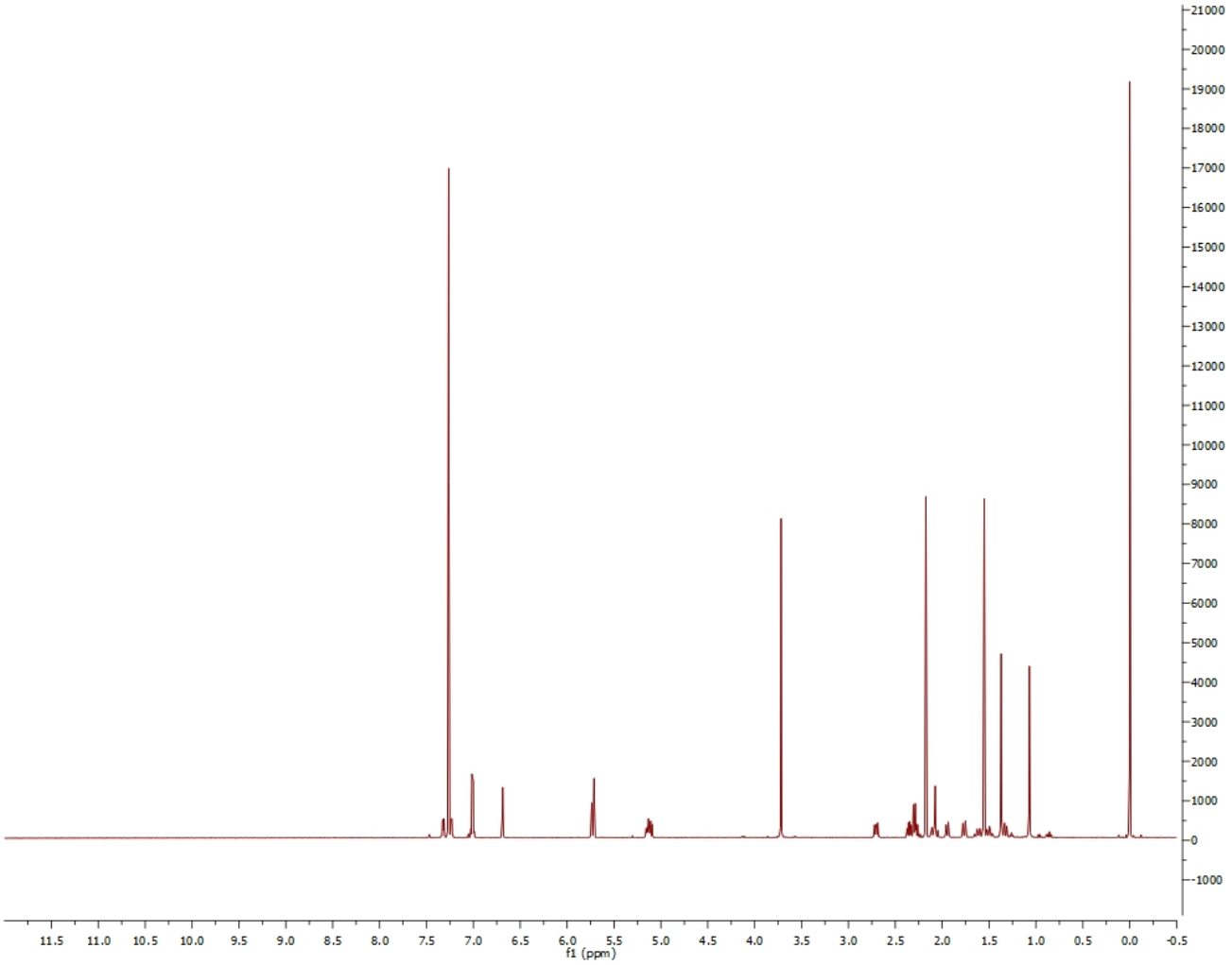

Figure S11. ^{1}H Spectrum of **7**.

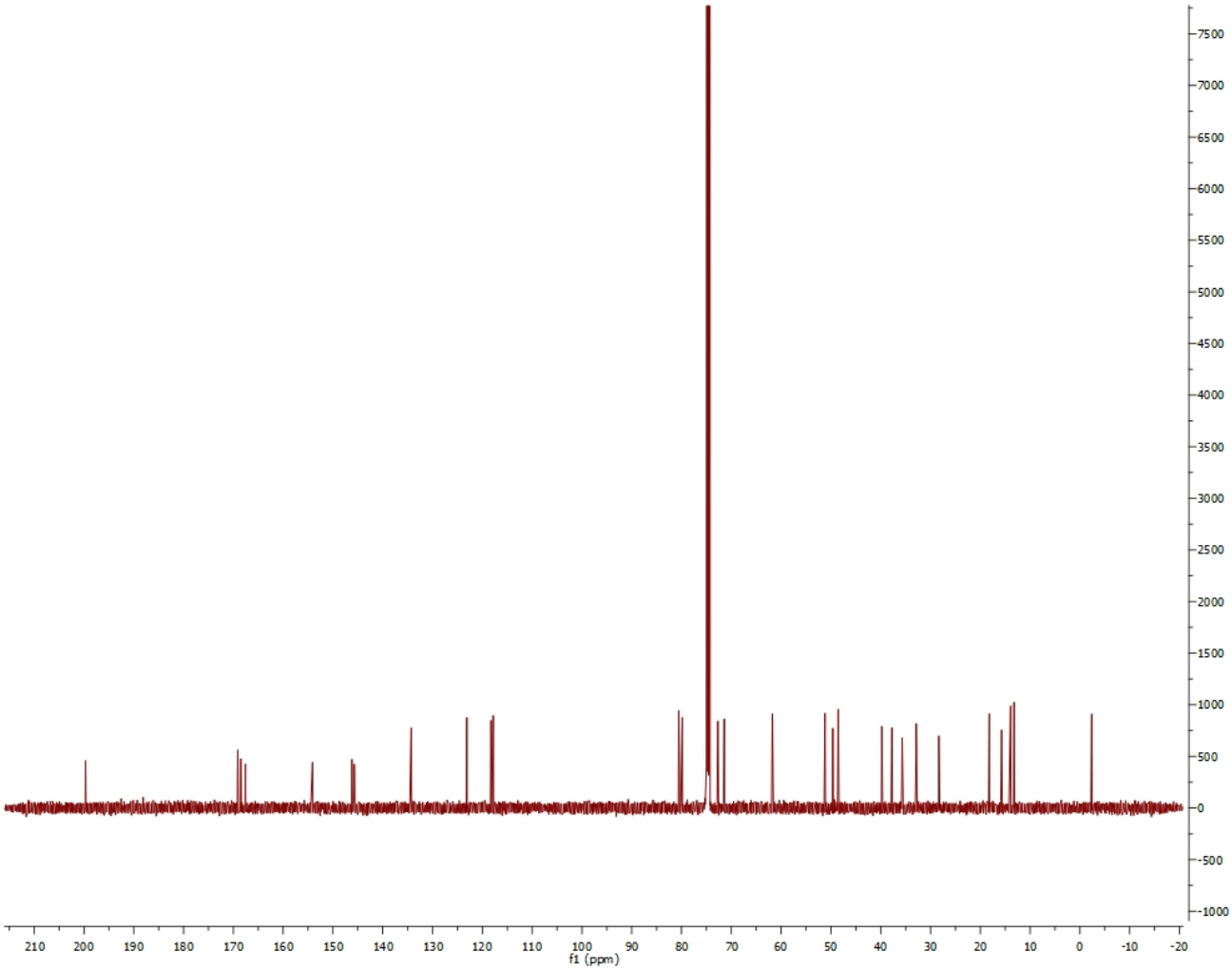

Figure S12. ^{13}C Spectrum of **7**.

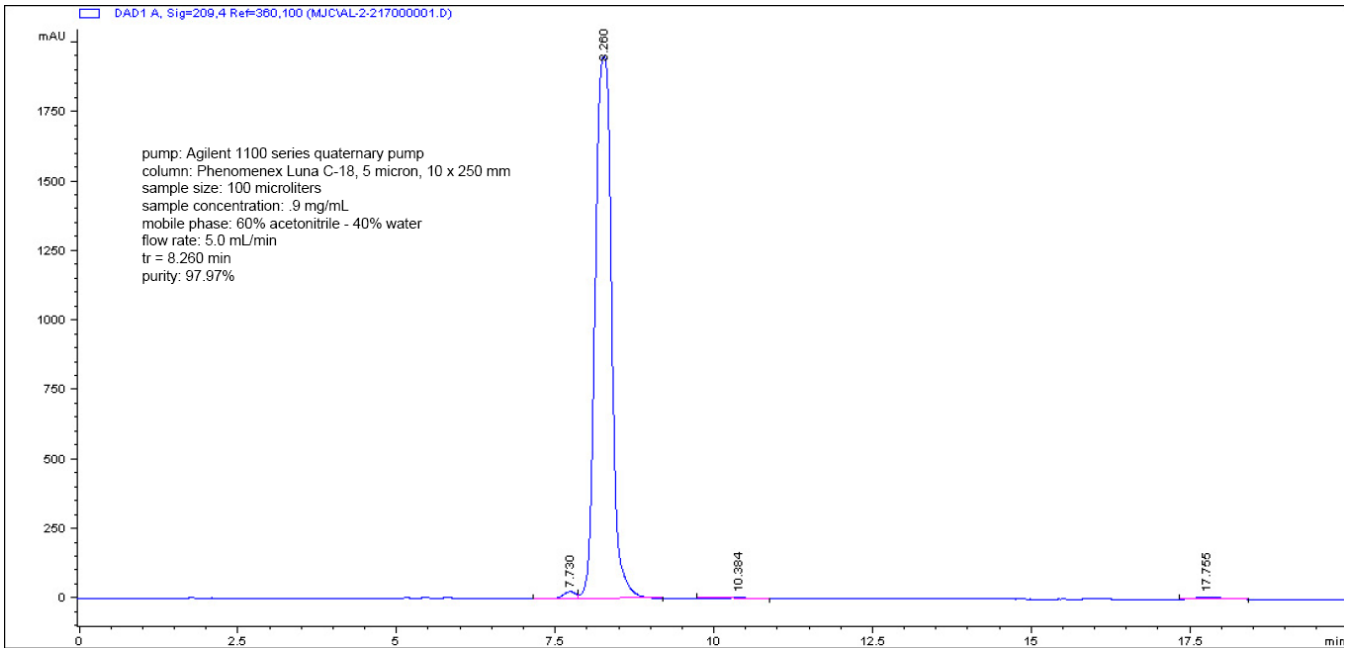

Figure S13. HPLC Analysis of **7**.

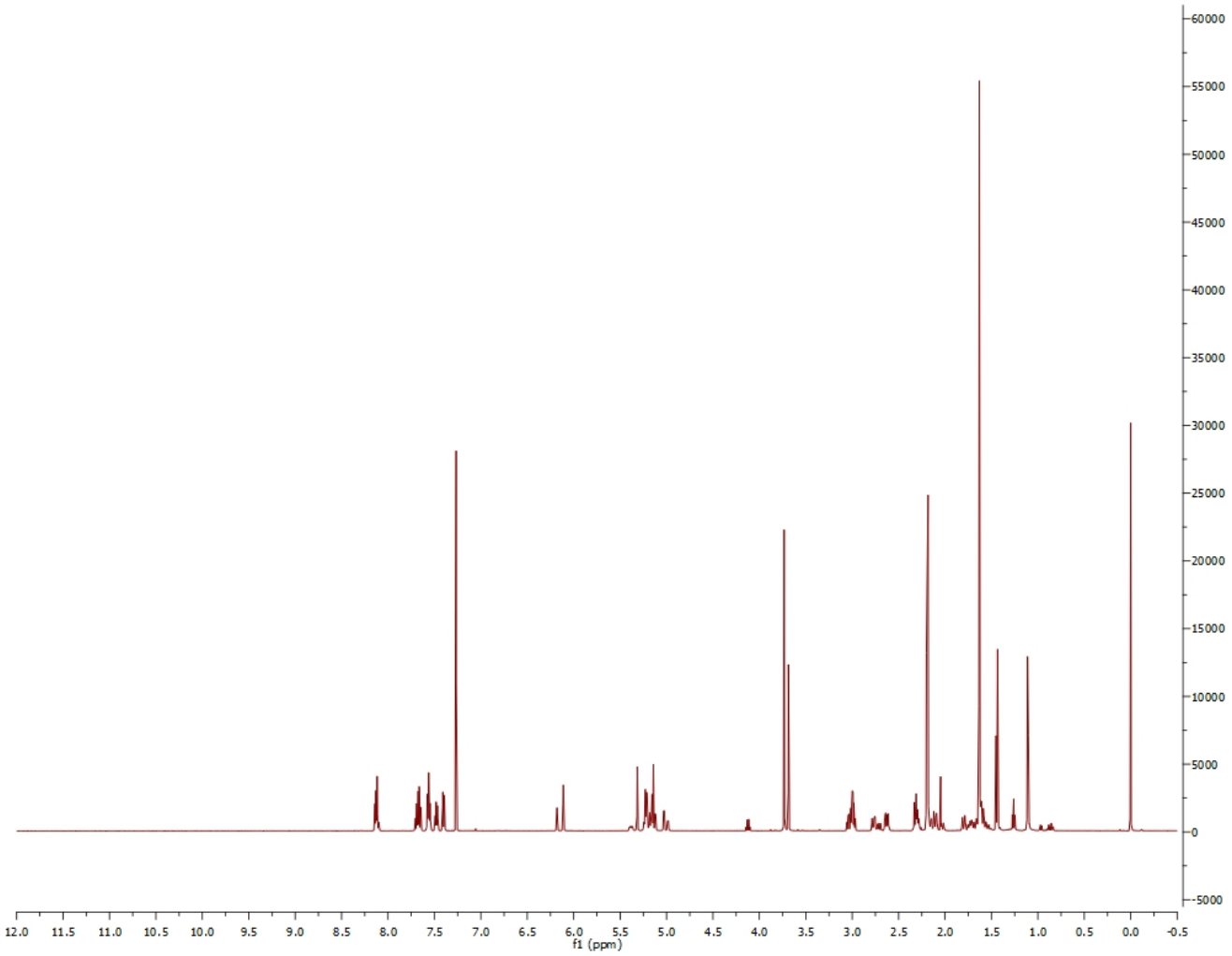

Figure S14. ^{1}H Spectrum of **11**.

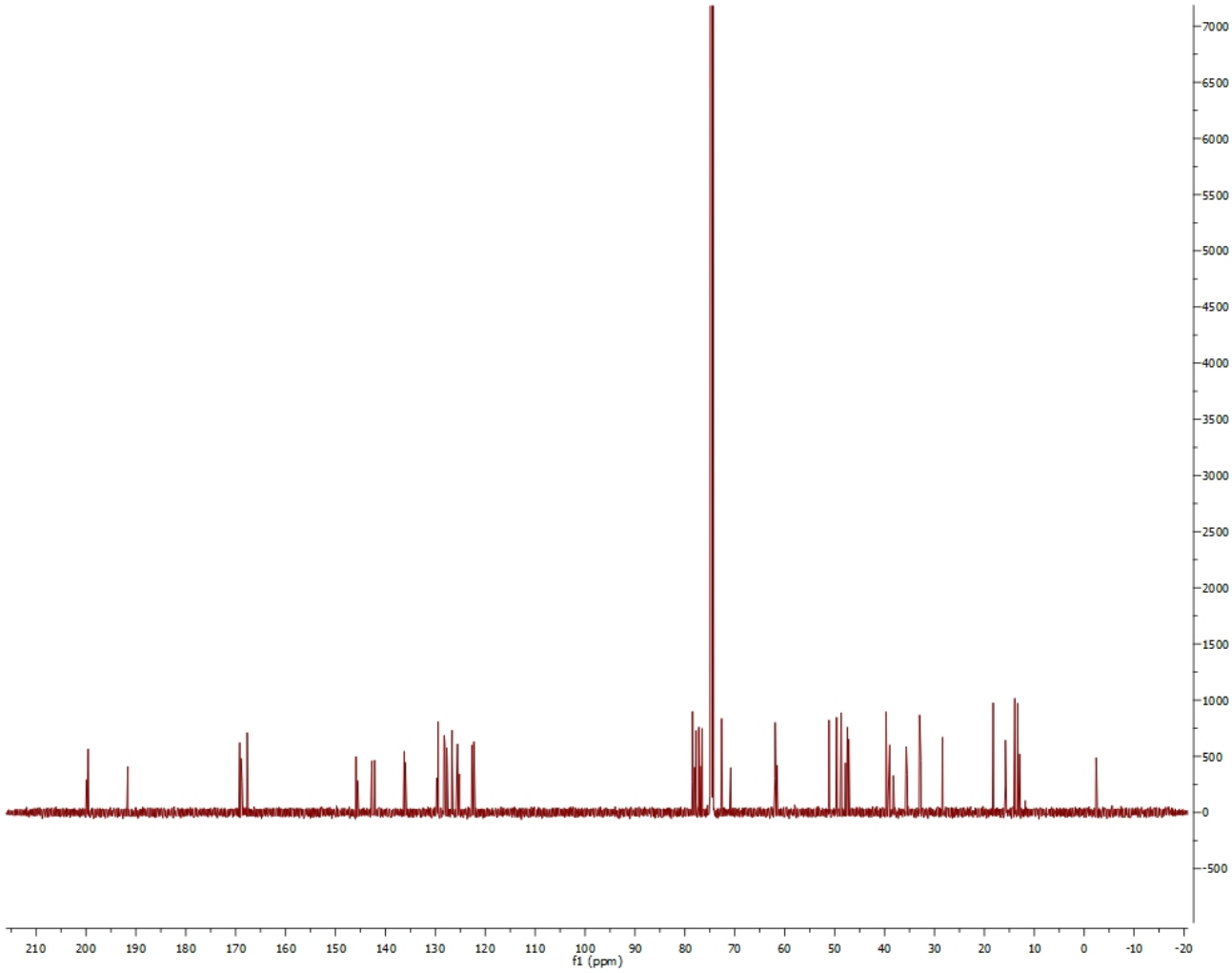

Figure S15. ^{13}C Spectrum of **11**.

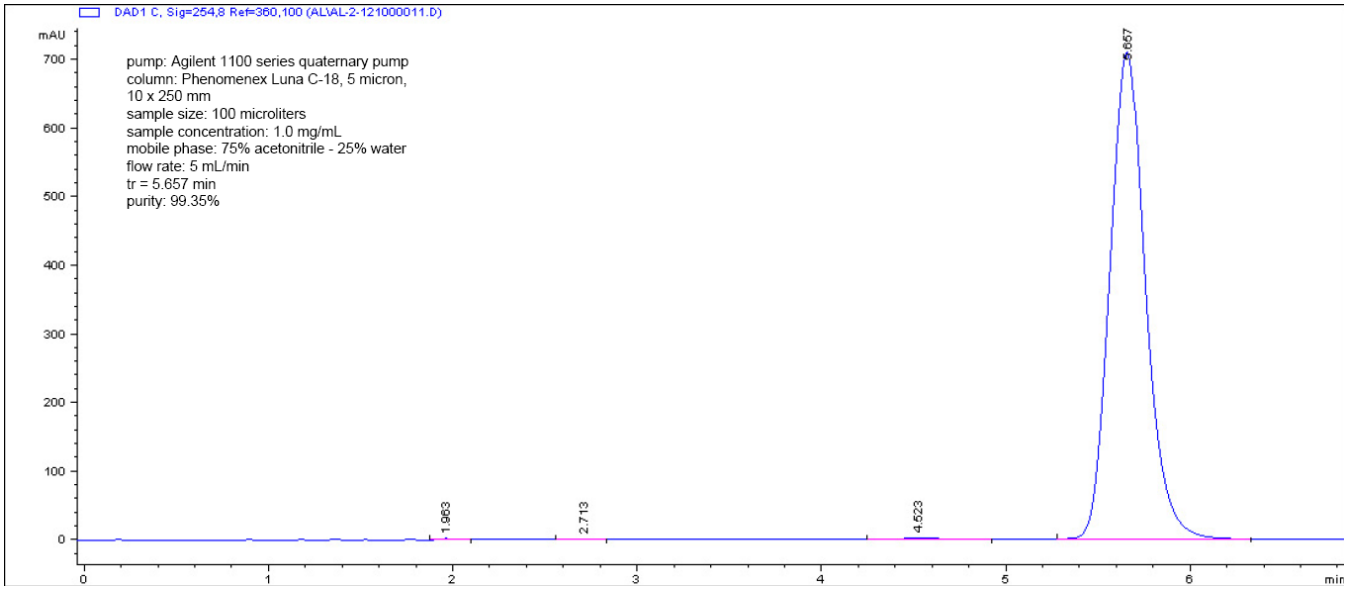

Figure S16. HPLC Analysis of **11**.

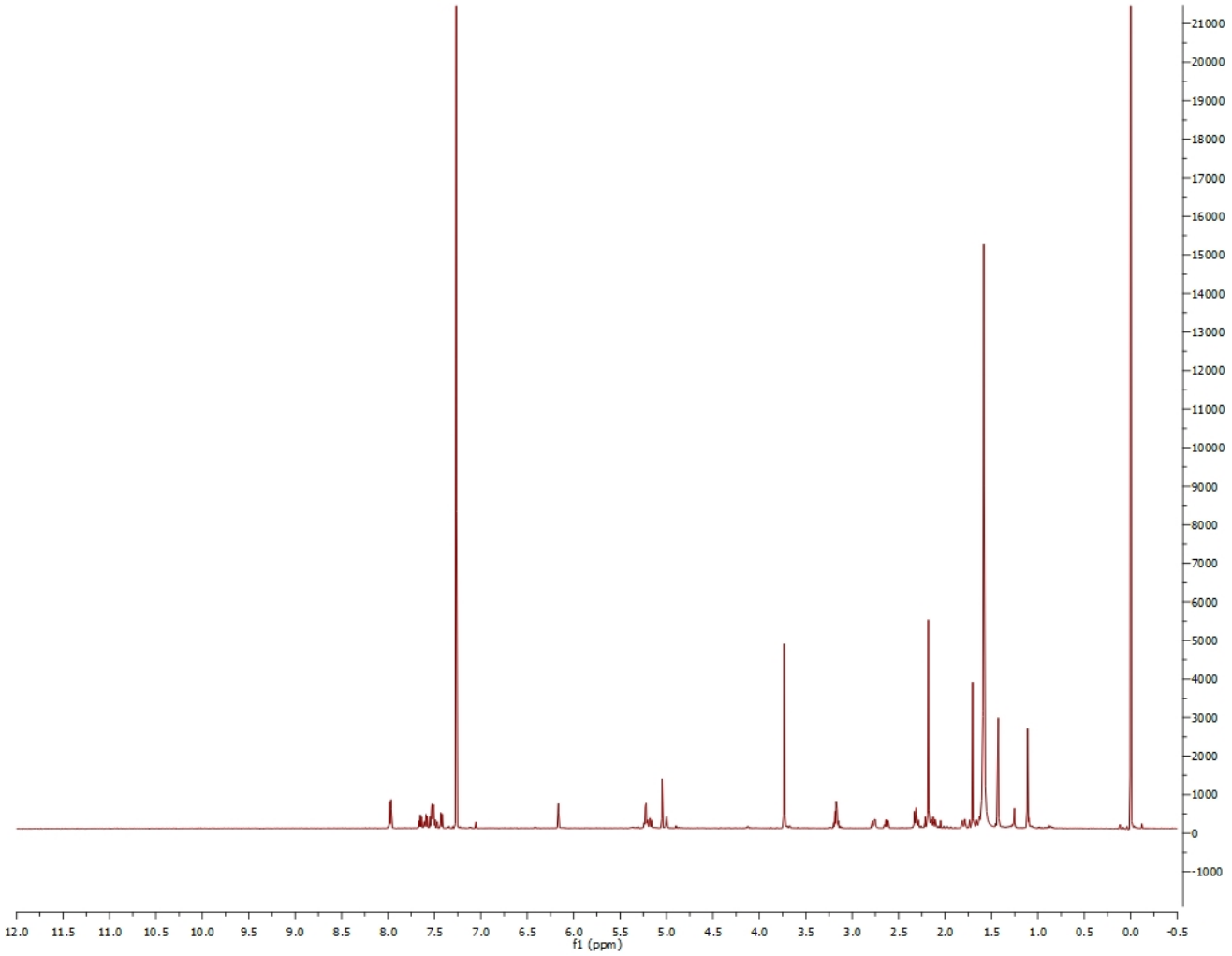

Figure S17. ^{1}H Spectrum of **12**.

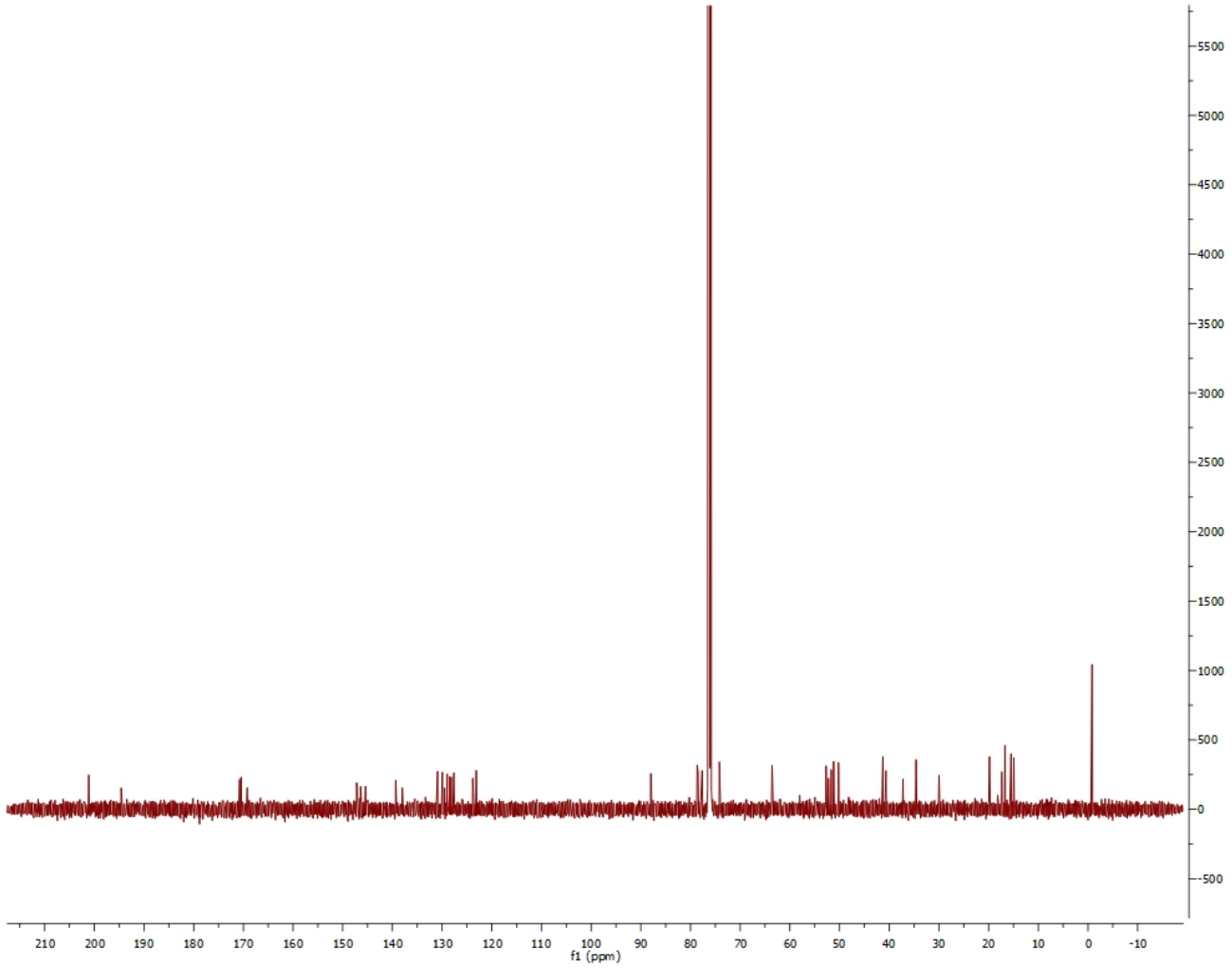

Figure S18. ^{13}C Spectrum of **12**.

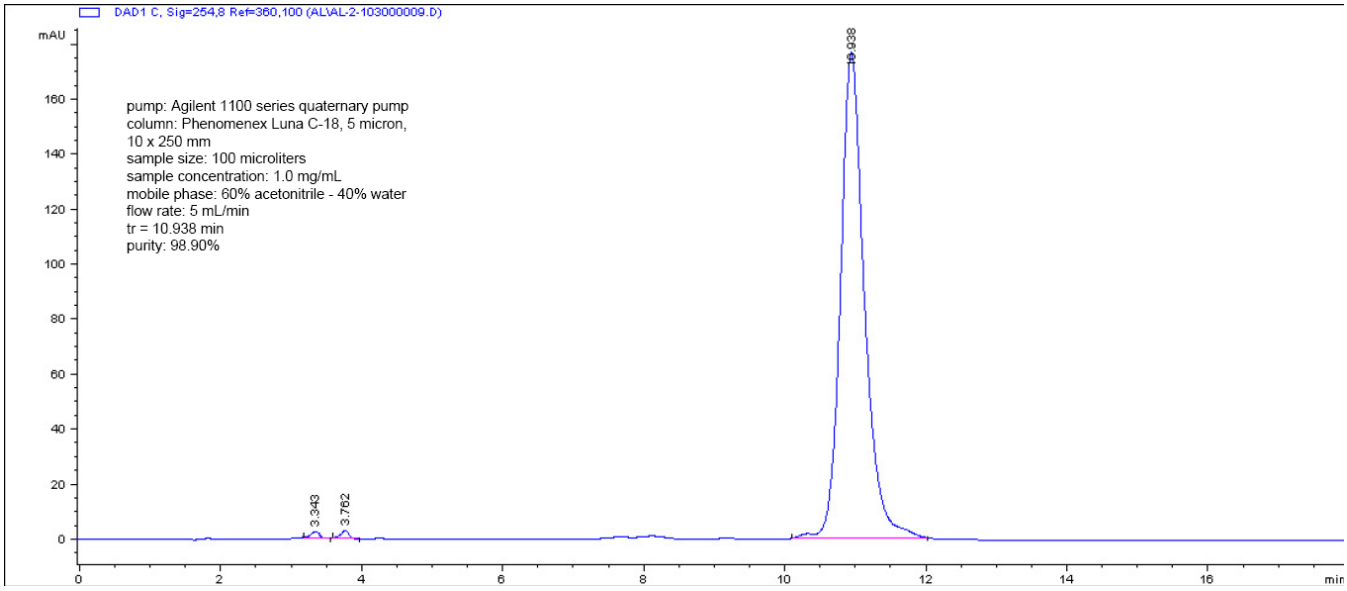

Figure S19. HPLC Analysis of **12**.

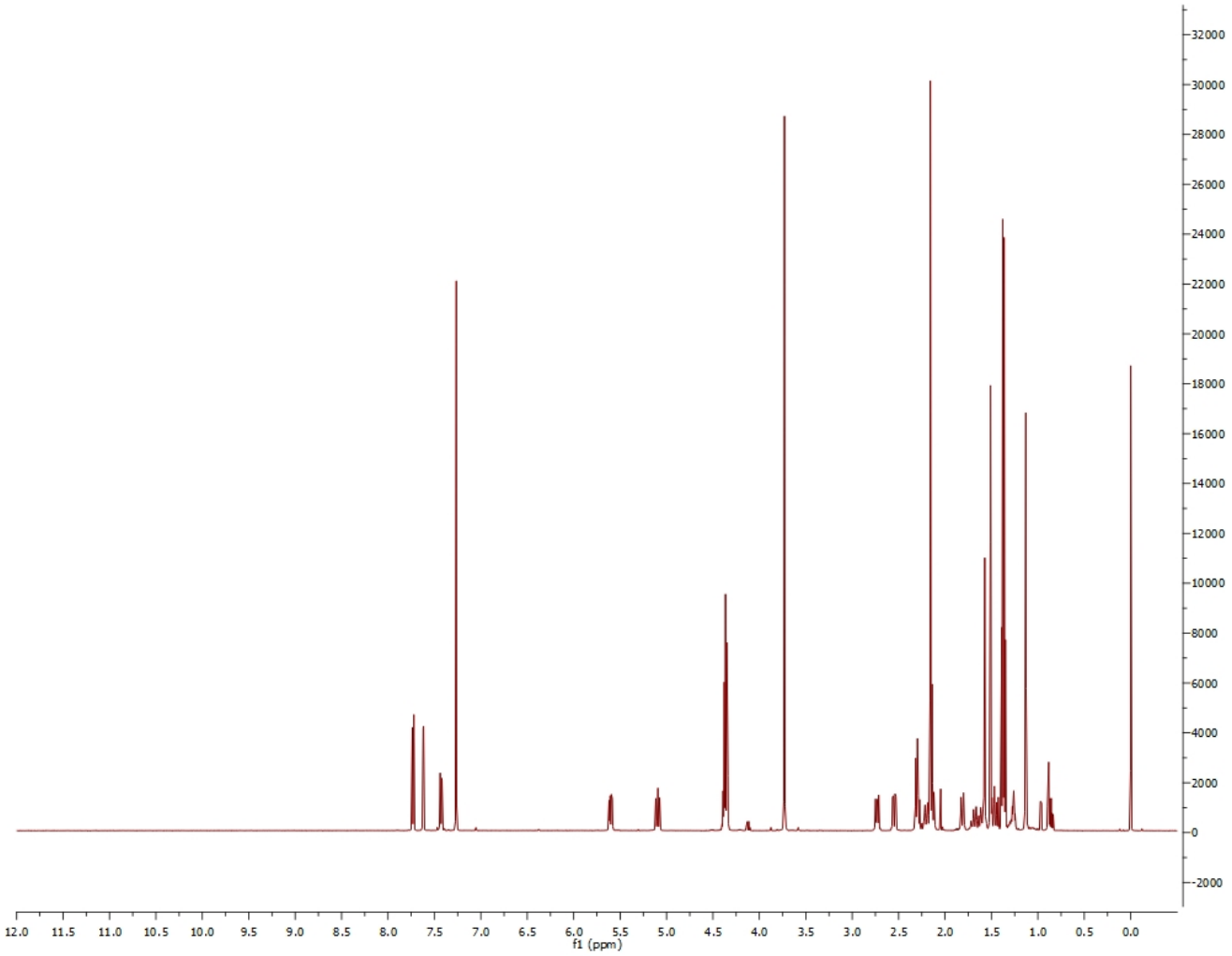

Figure S20. ^{1}H Spectrum of **13**.

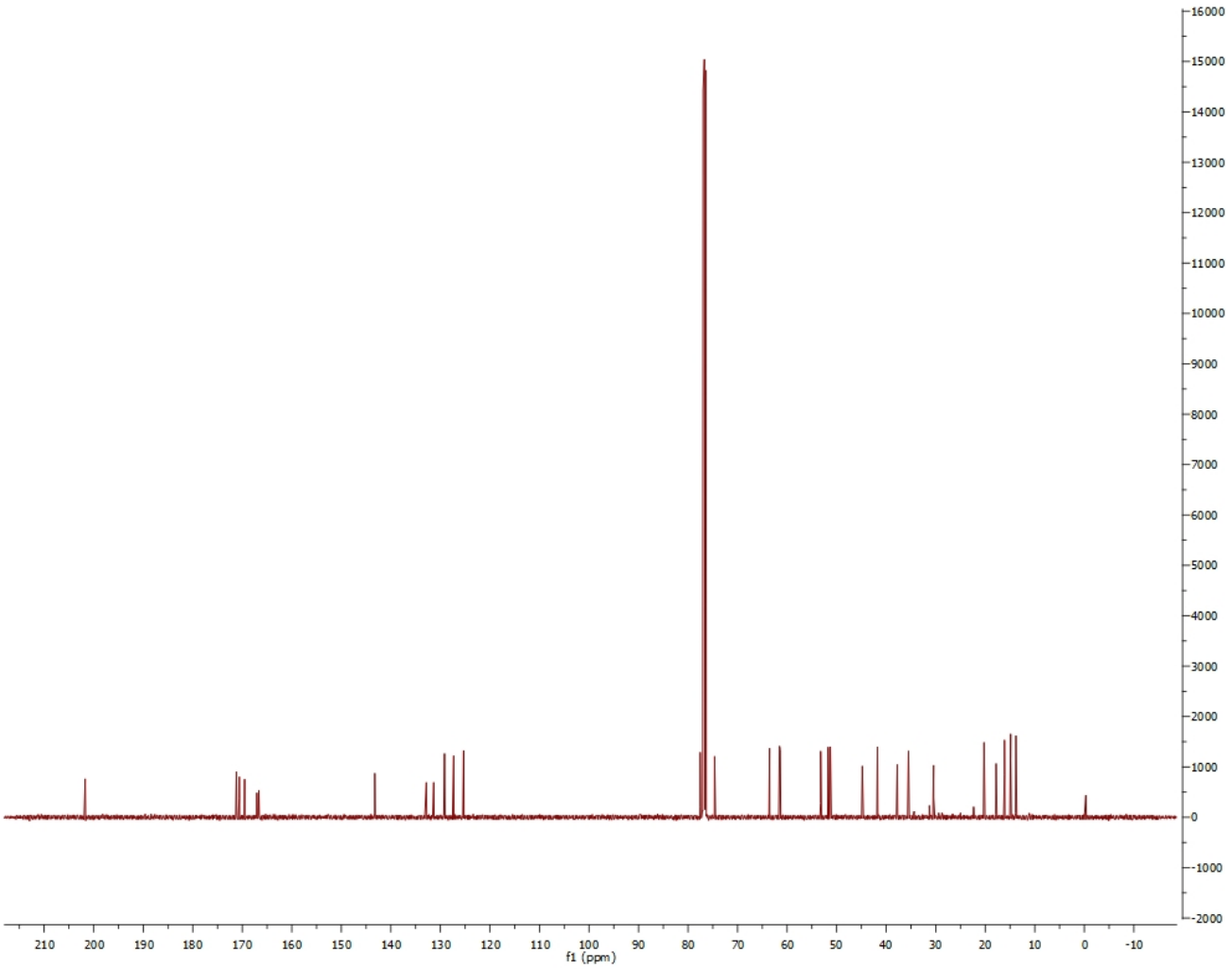

Figure S21. ^{13}C Spectrum of **13**.

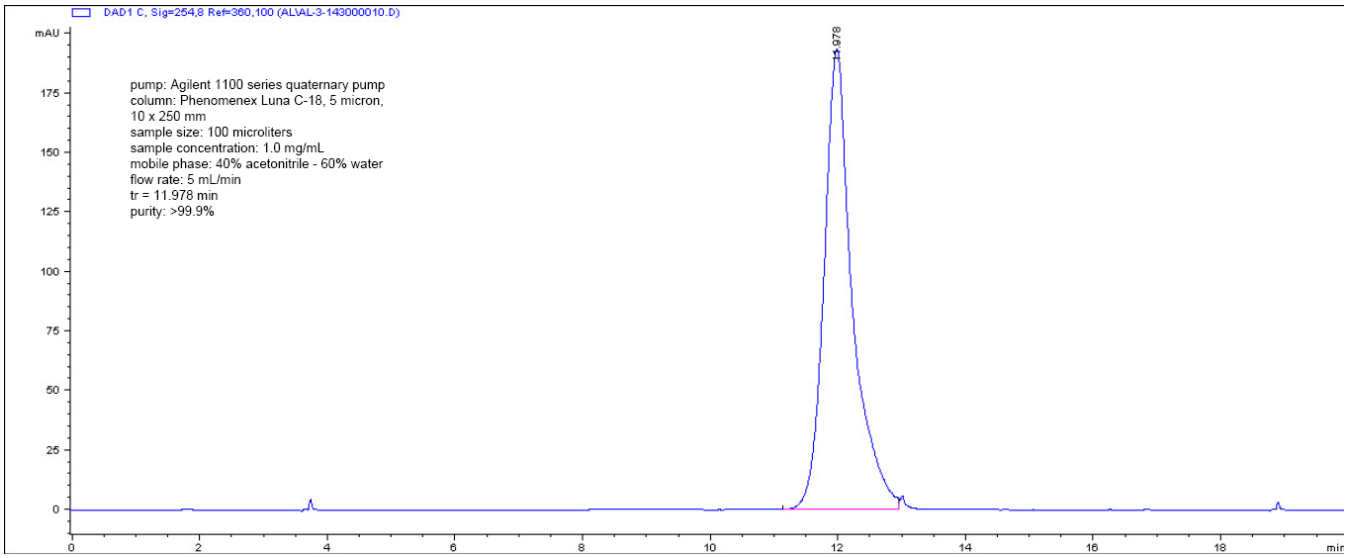

Figure S22. HPLC Analysis of **13**.

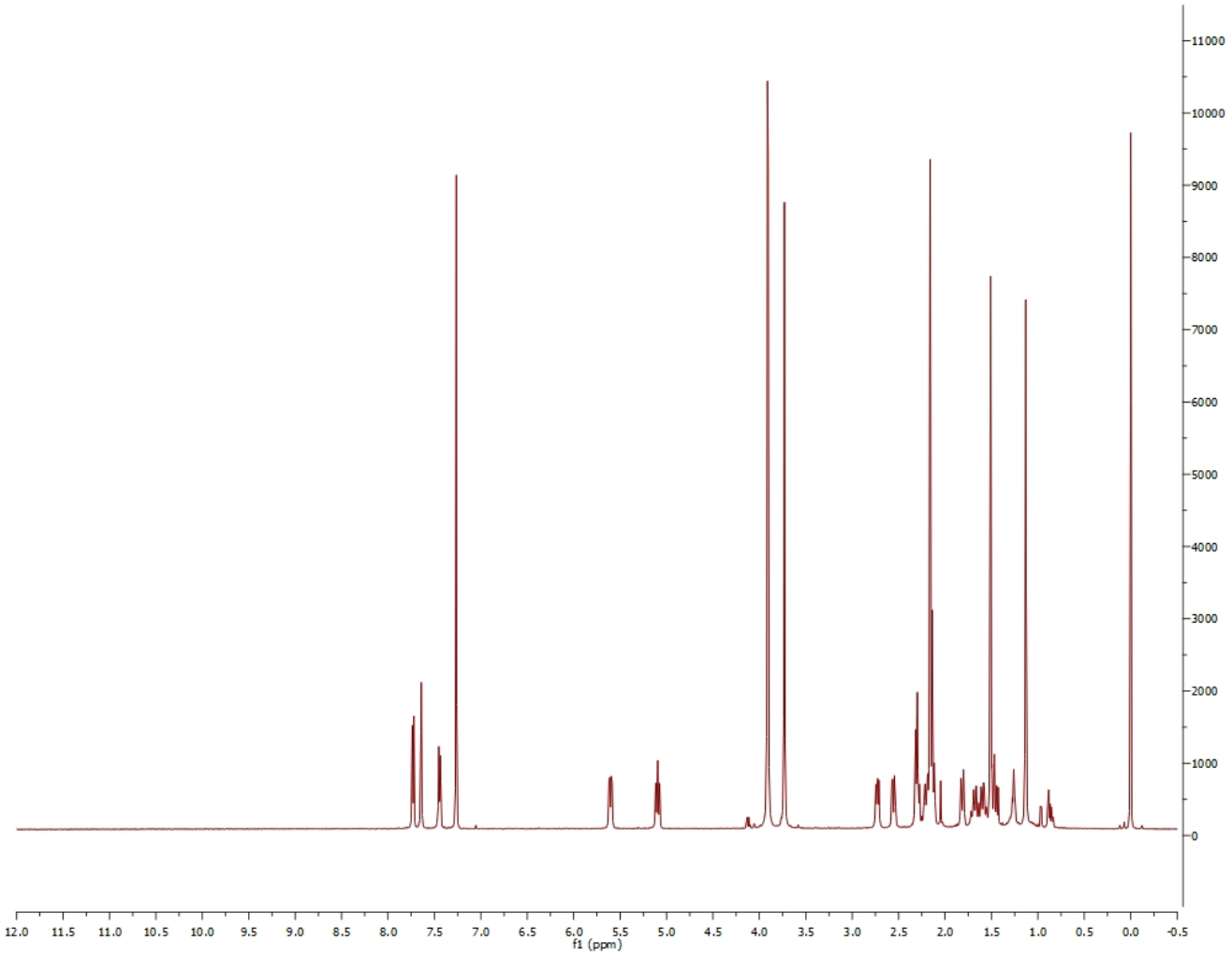

Figure S23. ^{1}H Spectrum of **14**.

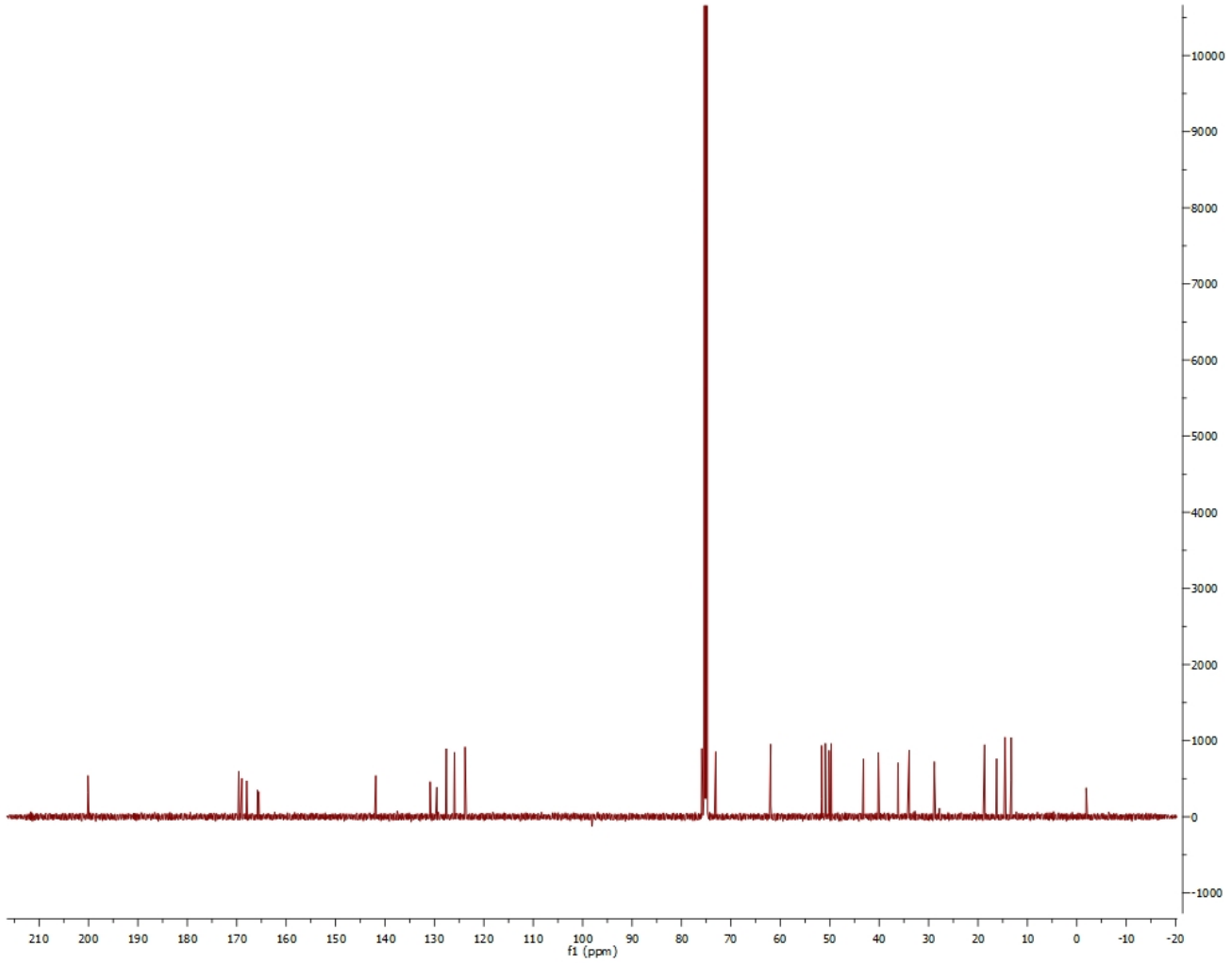

Figure S24. ^{13}C Spectrum of **14**.

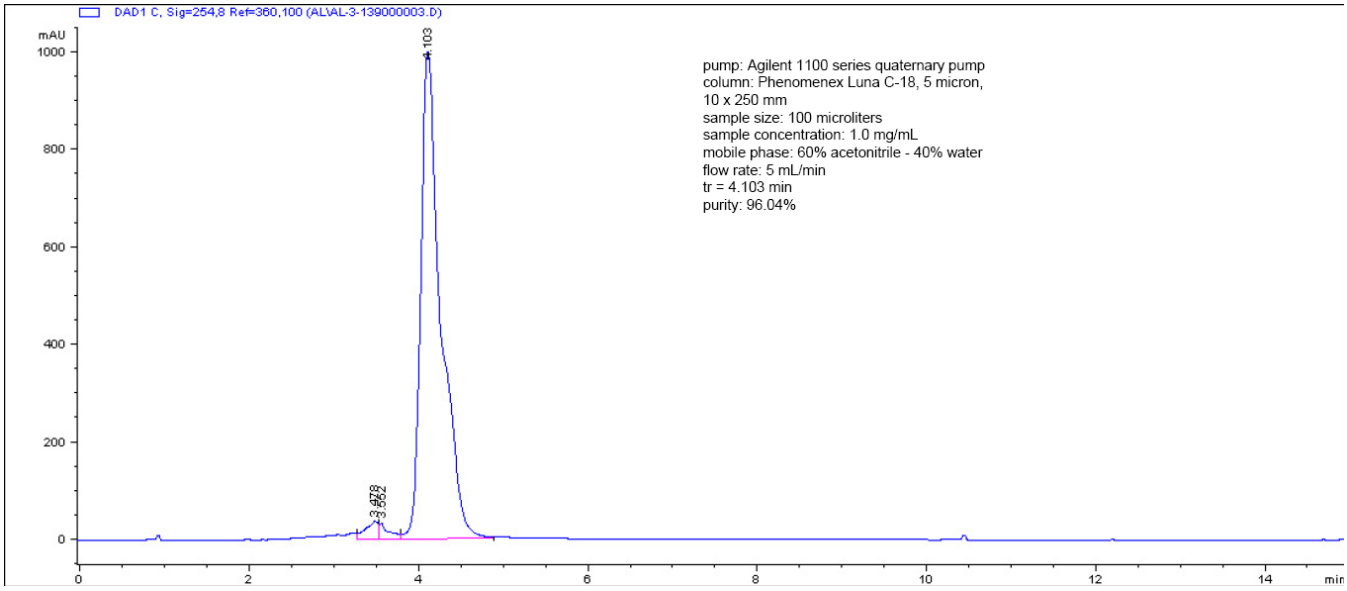

Figure S25. HPLC Analysis of **14**.

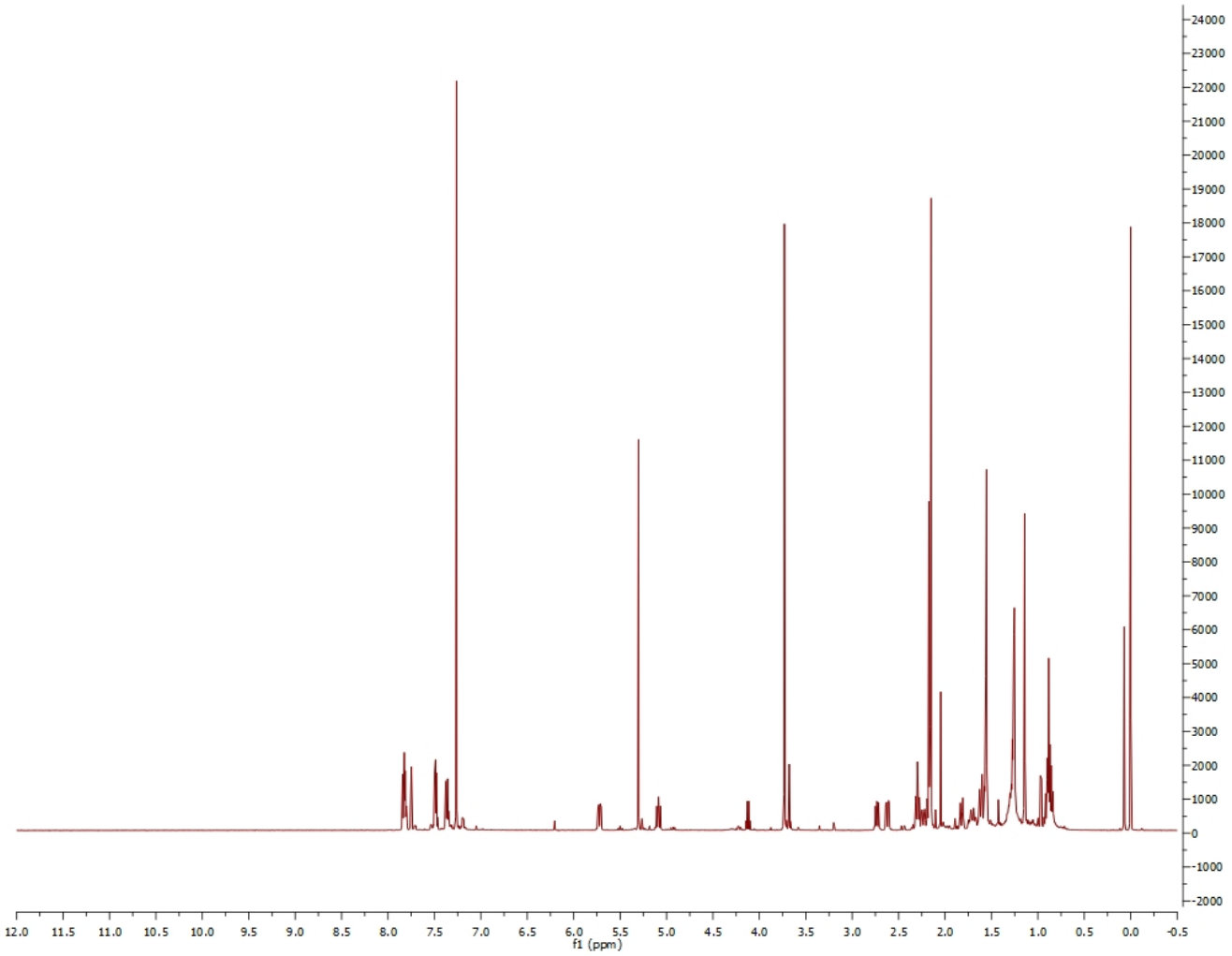

Figure S26. ^{1}H Spectrum of **15**.

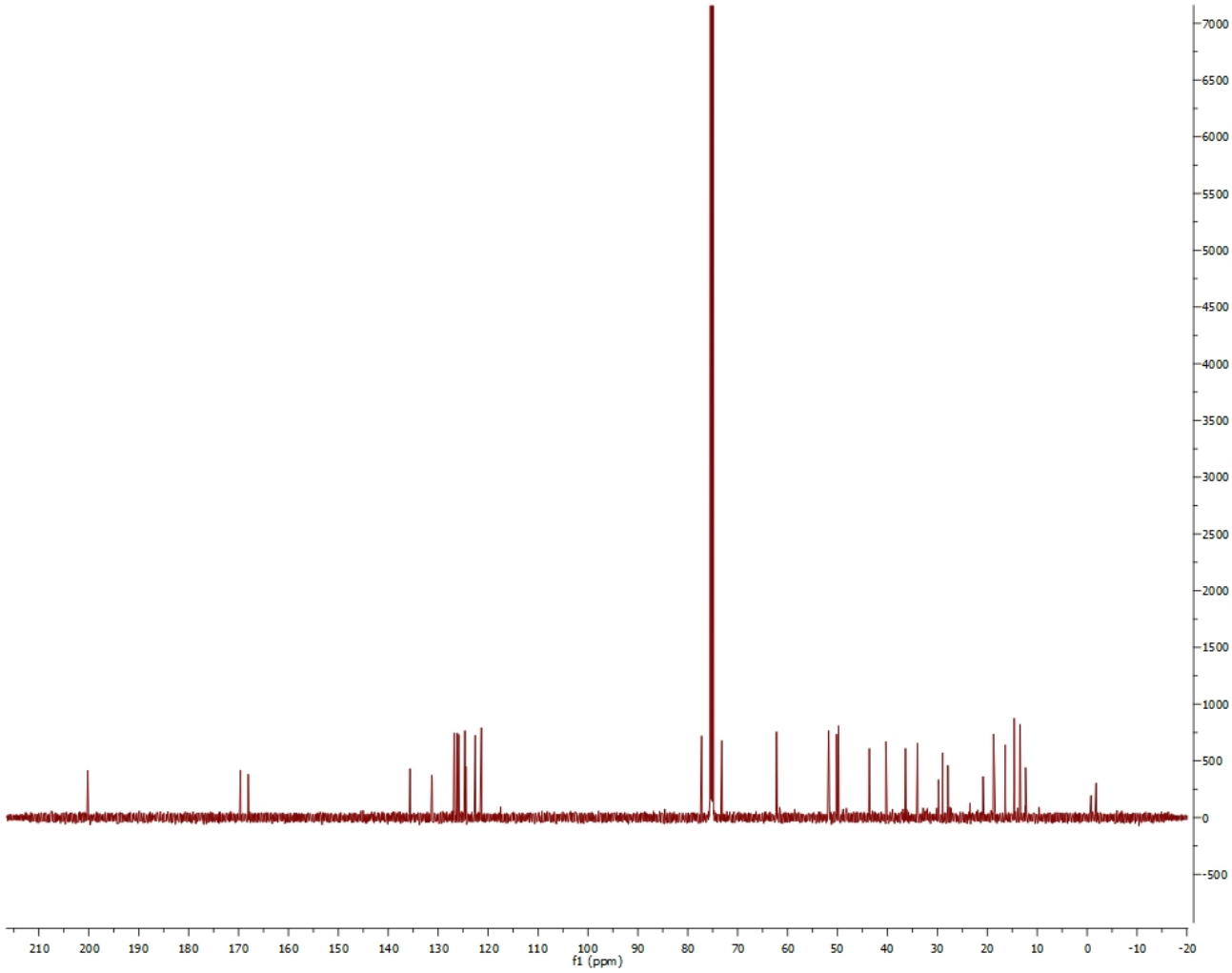

Figure S27. ^{13}C Spectrum of **15**.

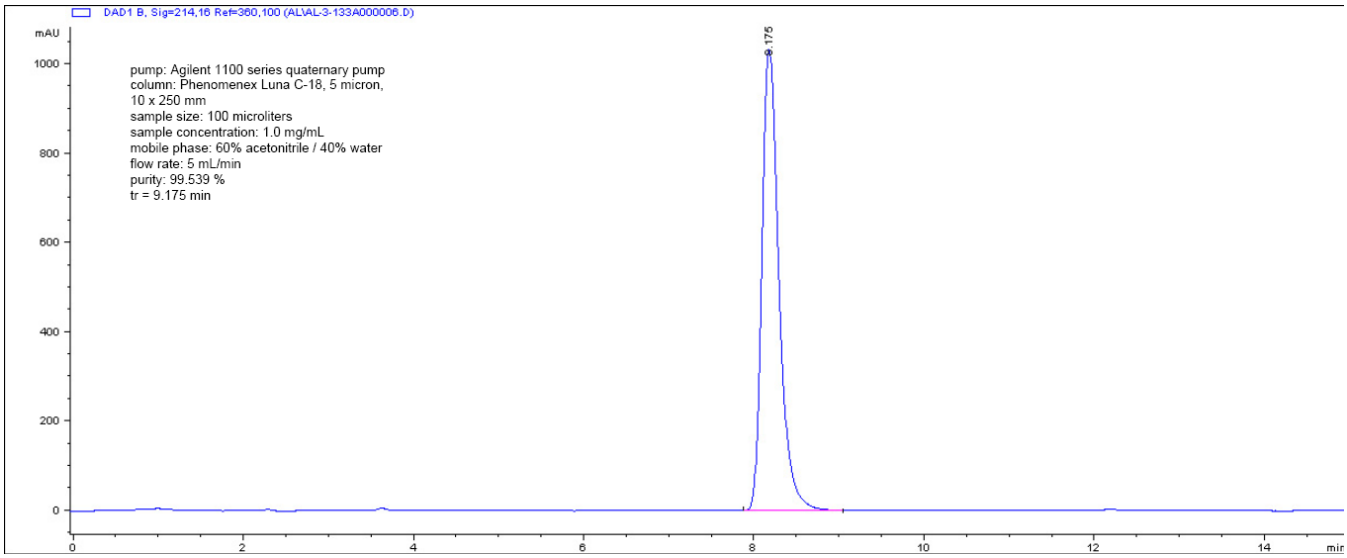

Figure S28. HPLC Analysis of **15**.

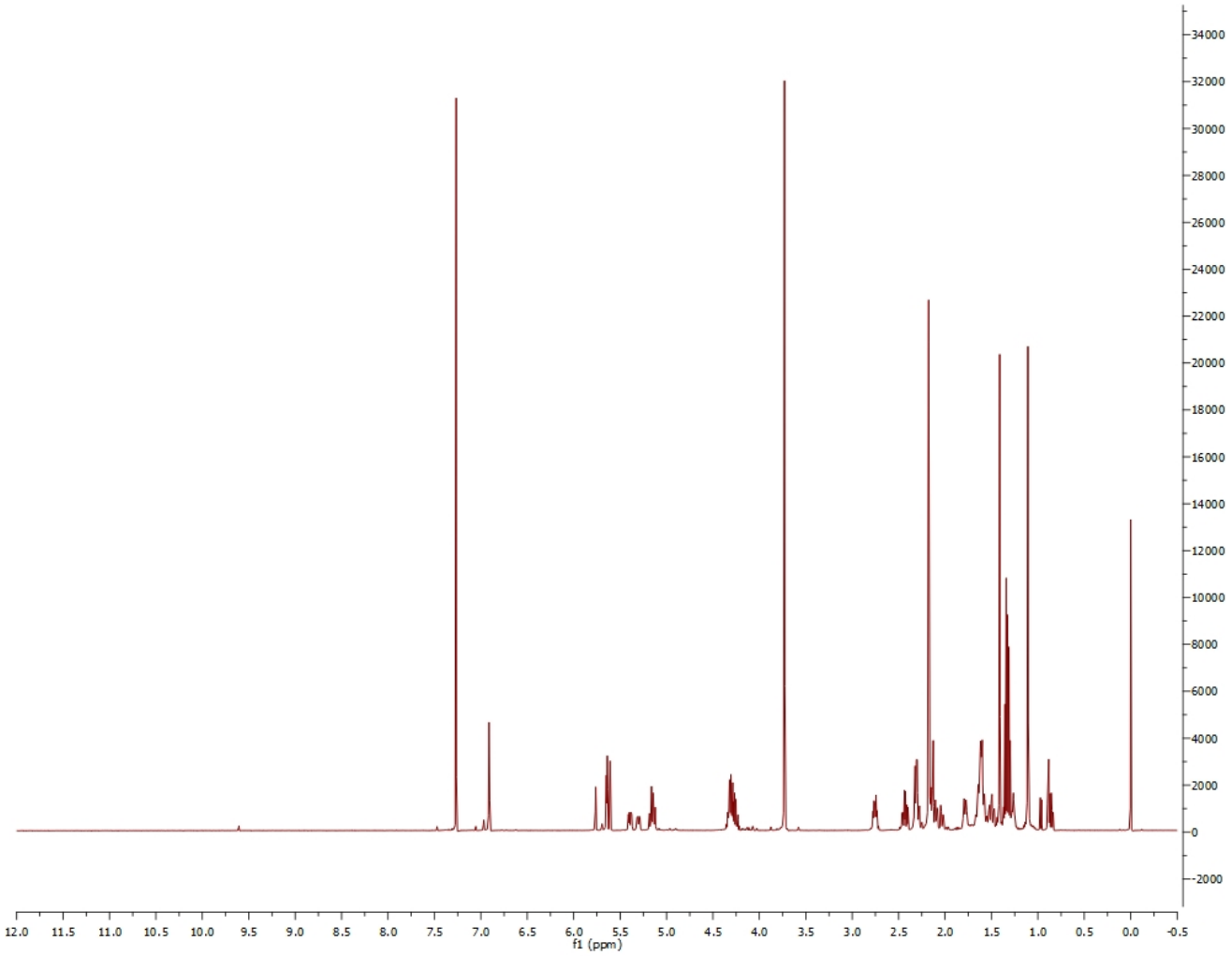

Figure S29. ^{1}H Spectrum of **16a/16b**.

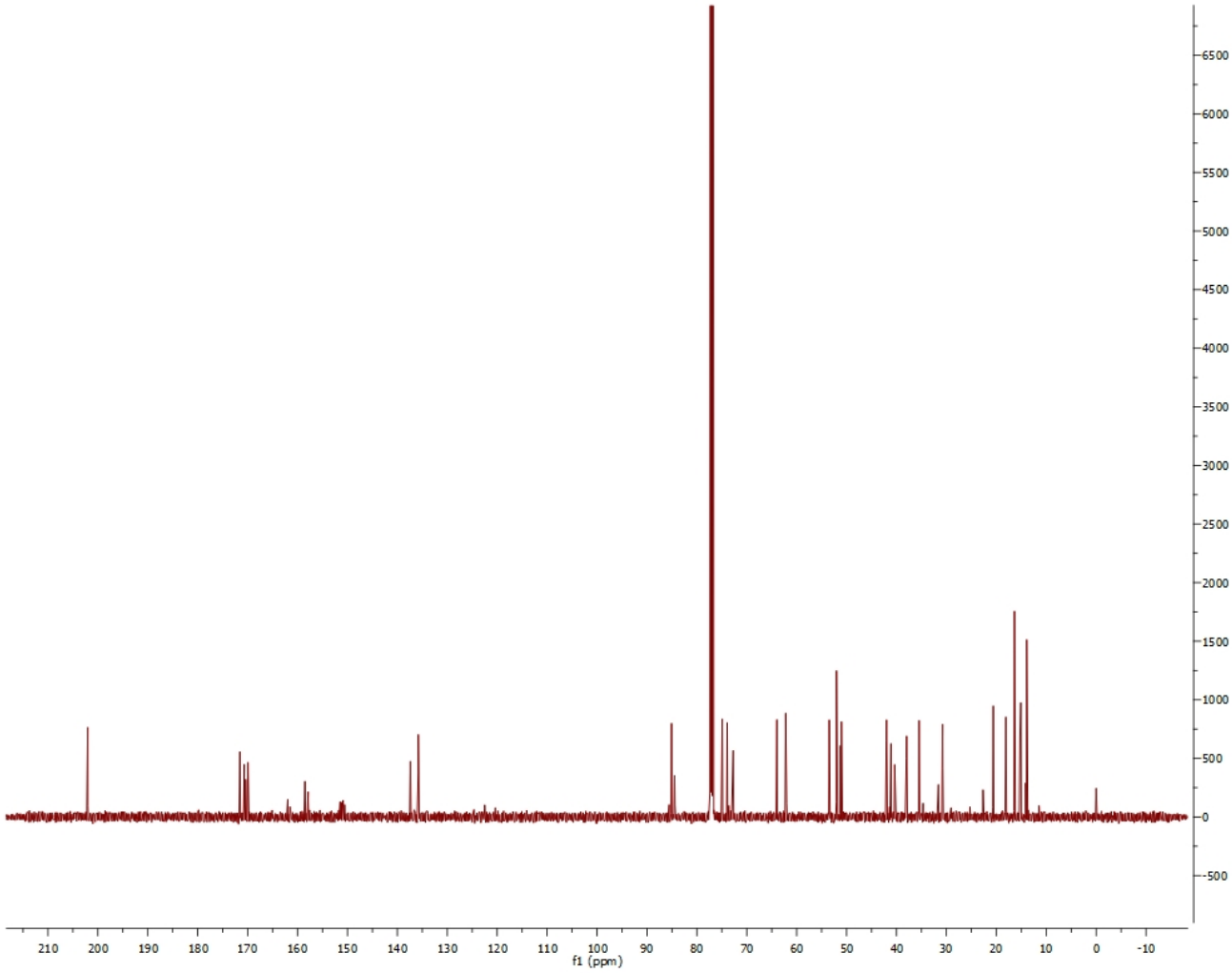

Figure S30. ^{13}C Spectrum of **16a/16b**.

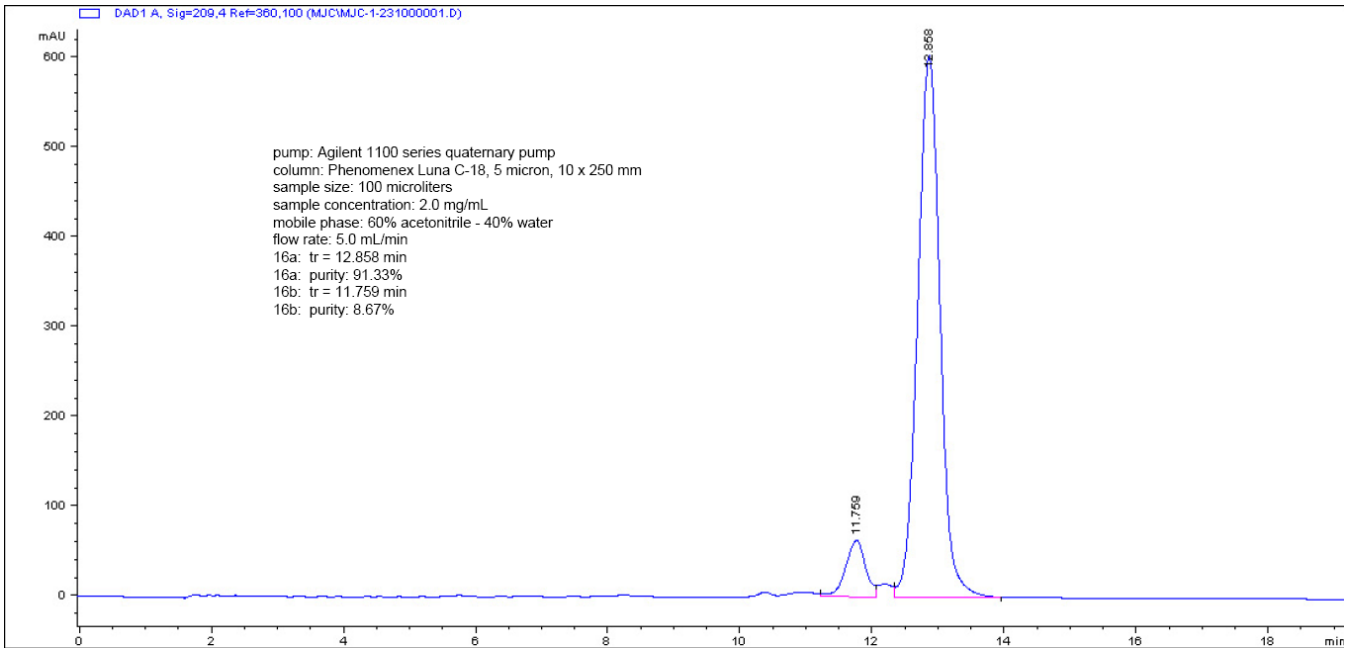

Figure S31. HPLC Analysis of **16a/16b**.

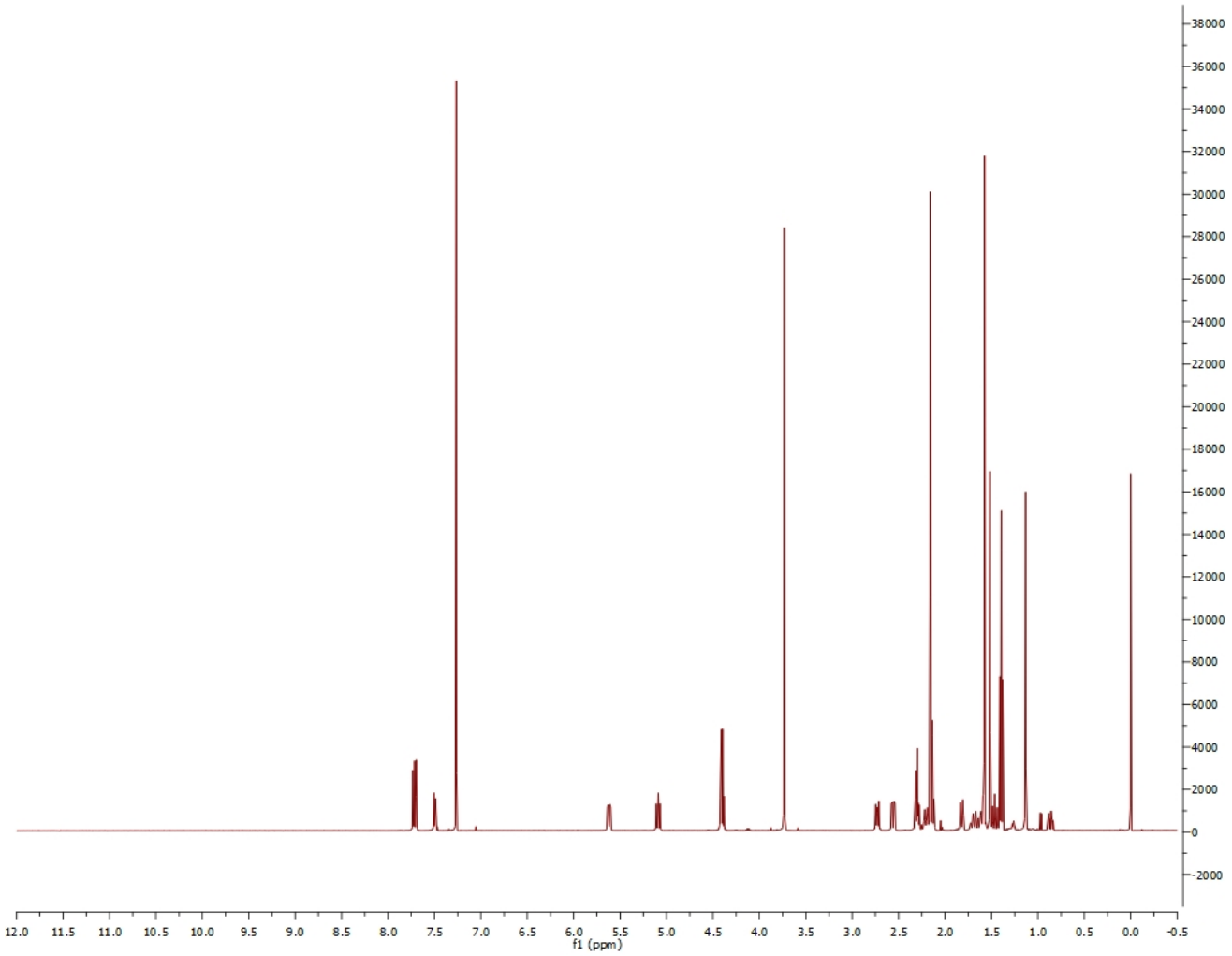

Figure S32. ^{1}H Spectrum of **17a**.

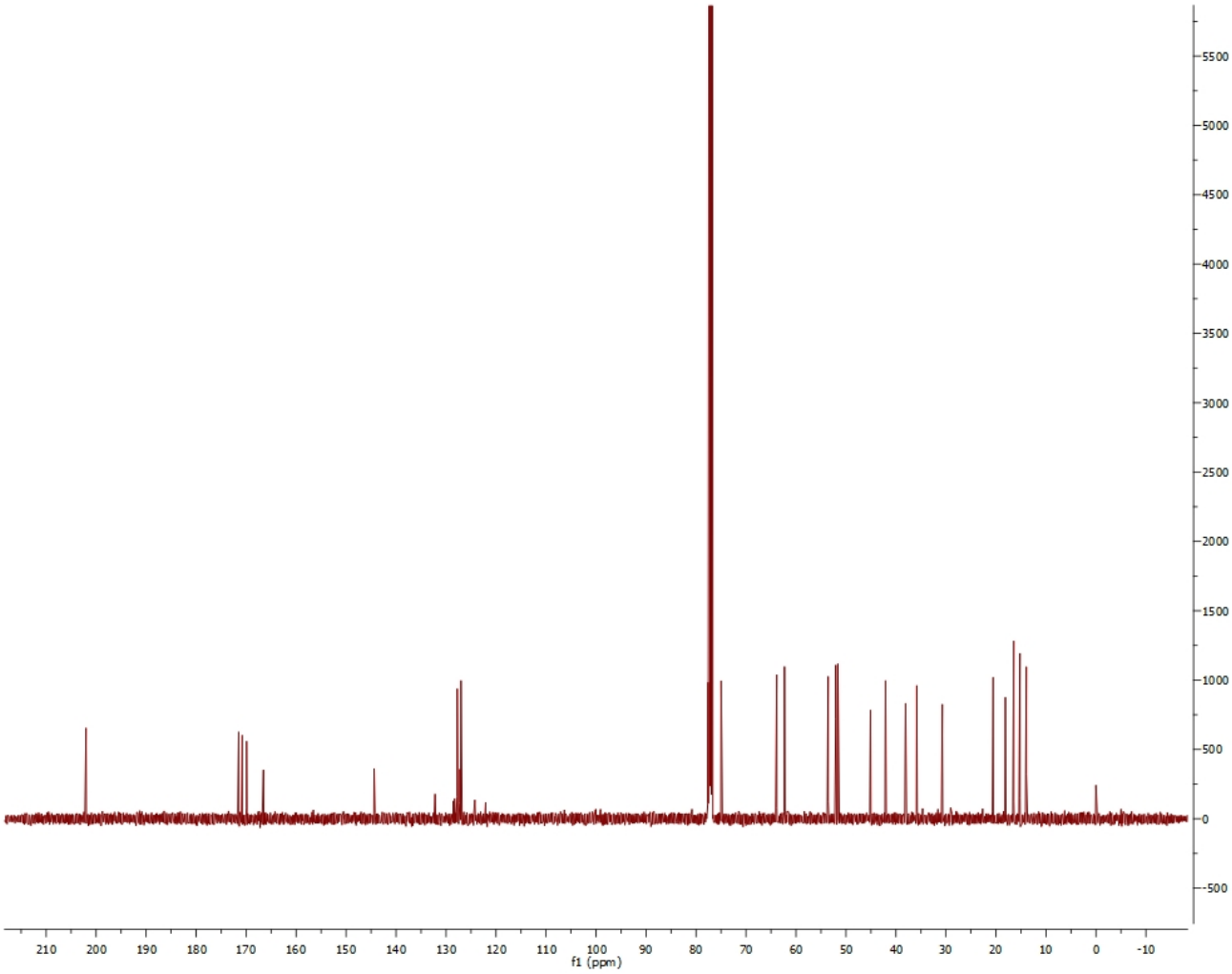

Figure S33. ^{13}C Spectrum of **17a**.

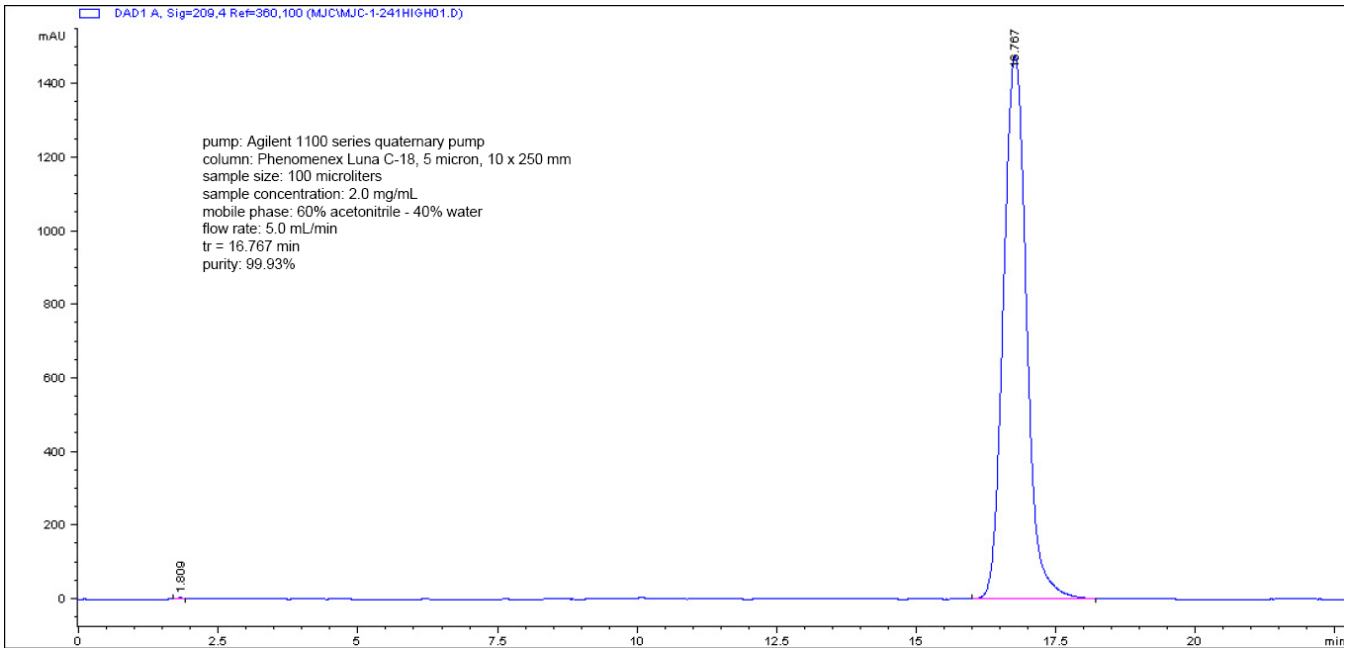

Figure S34. HPLC Analysis of **17a**.

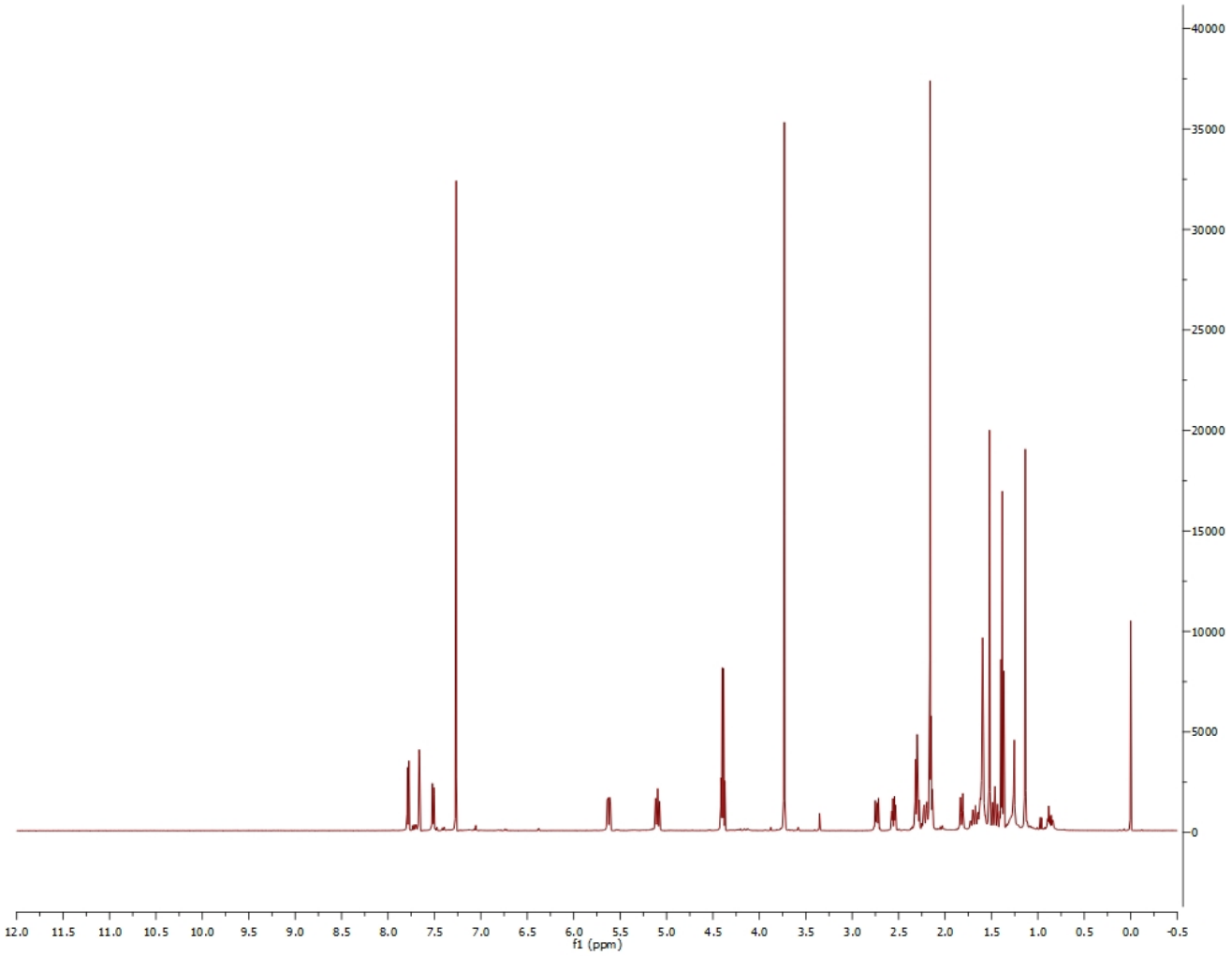

Figure S35. ^{1}H Spectrum of **17b**.

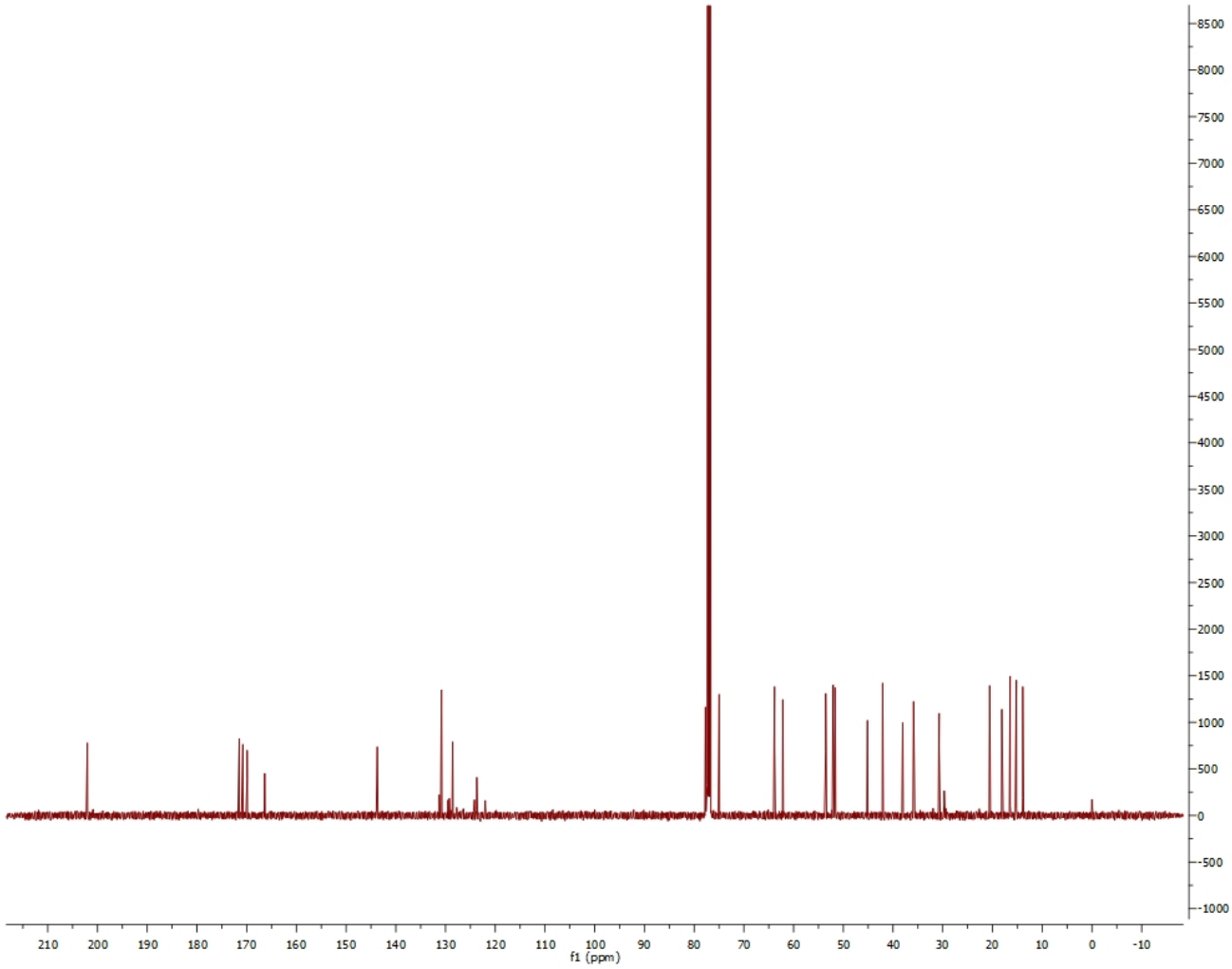

Figure S36. ^{13}C Spectrum of **17b**.

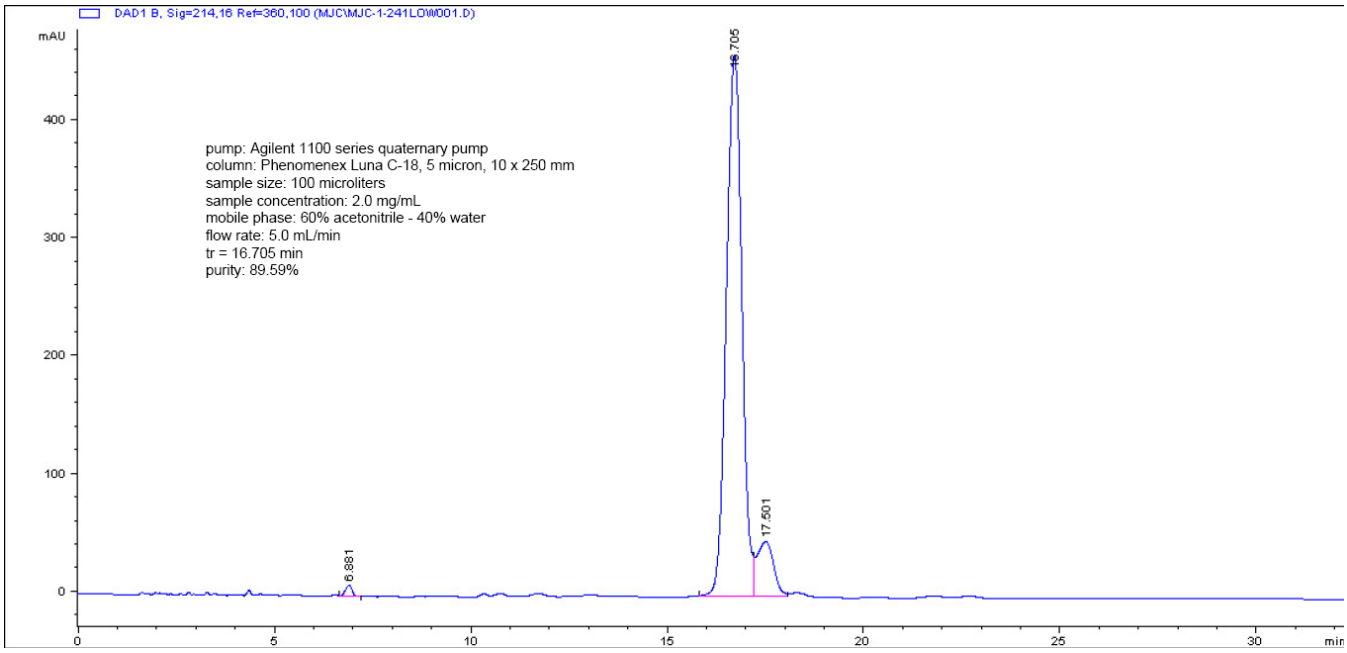

Figure S37. HPLC Analysis of **17b**.